Atmos. Chem. Phys. Discuss., https://doi.org/10.5194/acp-2017-969
Manuscript under review for journal Atmos. Chem. Phys.
Discussion started: 20 November 2017

Atmospheric Chemistry and Physics Discussions

LES study of the impact of moist thermals on the oxidative capacity of the atmosphere in southern West Africa

Fabien Brosse[1], Maud Leriche[1], Céline Mari[1], and Fleur Couvreux[2]

[1]Laboratoire d'Aérologie, Université de Toulouse, CNRS, UPS, France
[2]CNRM-GAME, Météo-France & CNRS, Toulouse, France

Correspondence to: Fabien Brosse (fabien.brosse@aero.obs-mip.fr)

Abstract. The hydroxyl radical (OH) is a highly reactive specie and plays a key role in the oxidative capacity of the atmosphere. The total OH reactivity, corresponding to the inverse of OH lifetime, may have a significant fraction non-attributable to commonly measured compounds. The turbulence-driven segregation of OH and its reactants can cause substantial modification of averaged reaction rates, and thus of the total OH reactivity, when compared to a perfectly mixed assumption. We study the impact of turbulent mixing on the OH reactivity with Large-Eddy Simulations from the Meso-NH model coupled on-line with a detailed chemistry mechanism in two contrasted regimes. Our findings show that the non-mixing of isoprene (resp. aldehydes) and OH leads to 30% decrease (resp. 16% increase) of the mean reaction rate at the top of the boundary layer and consequently to 9% decrease (resp. 5% increase) of the OH total reactivity in a biogenic (resp. anthropogenic) environment. Moreover, the total OH reactivity is highest inside thermals in both cases.

1 Introduction

The hydroxyl radical (OH) is an efficient cleansing molecule present in the troposphere. It is mainly produced during daytime through the reaction of water vapor with $O(^1D)$, formed by the ozone photolysis, while nitrogen oxides and volatile organic compounds (VOC) are its major sinks. OH has a very high reactivity and reacts with numerous chemical species, controlling their chemical lifetimes (Ehhalt, 1999). Several field campaigns have been conducted to study the total OH reactivity for urban or forested environments. The measured reactivity have been compared to the calculated reactivity, obtained by the sum of OH reactants concentrations multiplied by their reaction constants. A missing part, corresponding to the difference in measured and calculated OH reactivity, is found under urban or biogenic conditions but also in clean remote regions. OH reactivity measurements made in urban areas proved to be in agreement (less than 10%) with the calculated OH reactivity in New York (Ren, 2003), in Houston (Mao et al., 2010) or in a urban controlled environment (Hansen et al., 2015b). However, discrepancies in urban areas have been noticed between the measured and the calculated OH reactivity in Nashville (Kovacs et al., 2003) (35% less for the calculated reactivity), in Mexico (Shirley et al., 2006) (25%) or in Tokyo (Sadanaga, 2004) (25%). The

Atmos. Chem. Phys. Discuss., https://doi.org/10.5194/acp-2017-969
Manuscript under review for journal Atmos. Chem. Phys.
Discussion started: 20 November 2017

Atmospheric Chemistry and Physics Discussions

differences between the measured and the calculated total OH reactivity are higher in forested areas. Di Carlo (2004) found a missing fraction of 50% in OH reactivity during the PROPHET campaign in Michigan. These results are comparable to the missing part (50 to 58%) calculated from measurements made in a boreal forest in Finland (Sinha et al., 2010; Nölscher et al., 2012). Similarly, Nölscher et al. (2016) calculated an accounted fraction of OH reactivity close to 49% in an amazonian rainforest.

As addressed by Williams and Brune (2015), atmospheric models do not correctly simulate the observed total OH reactivity. Attempts to use box models with detailed chemical mechanism or 3D-models with coarse resolution to fill the gap in OH reactivity proved to be insufficient but the reasons still remain unclear. This could be partly due to not yet discovered OH reactions pathways, and thus not implemented in atmospheric models. OH recycling during the isoprene oxidation chain in forest environments characterized by lox NO_x conditions was proposed to explain the uncertainties in the simulated HO_x budget (Lelieveld et al., 2008; Butler et al., 2008; Peeters et al., 2009; Pugh et al., 2010; Stone et al., 2011). However, Stone et al. (2011) studied several proposed OH recycling mechanism present in the literature and found that biases from OH and HO2 concentrations still exist whatever the mechanism. One possible issue in the total OH reactivity retrieval not mentioned by previous studies could lie in neglecting the turbulent motions in the transport of chemical compounds in the boundary layer, which can segregate chemical species and reduce the mean reaction rate.

The atmospheric boundary layer has a turbulent structure characterized by strong and narrow updrafts surrounded by weak and large descending areas (Molemaker and Vilà-Guerau de Arellano, 1998; Schumann, 1989). Considering passive scalars, Wyngaard and Brost (1984) found that the surface bottom-up transport is more important to the vertical diffusion than the entrainment zone top-down transport in a convective boundary layer. Updrafts in the boundary layer create a spatial discrimination of pollutants concentrations between thermals and their environment. This heterogeneity in chemical species redistribution influence the mean reaction rate obtained considering averaged reactants concentrations (Vilà-Guerau de Arellano and Cuijpers, 2000). By an idealized simulation, Molemaker and Vilà-Guerau de Arellano (1998) have shown that, for a second-order reaction implying a top-down and a bottom-up species, reaction rates are maximum in updrafts near the surface and in downdrafts at the top of the boundary-layer. Ouwersloot et al. (2011) studied the inefficiency of turbulent mixing over heterogeneous surfaces and found that the highest reaction rates for isoprene and OH are located in thermals at the top of the boundary layer. The chemical reactivity of boundary layer is then determined by the ability of turbulence to mix reactive species (Molemaker and Vilà-Guerau de Arellano, 1998).

Vertical motions associated with clouds and sea-breeze impact the atmospheric chemistry and pollution levels near the surface since they dilute the chemical species and increase the upward transport of surface emissions (Chen et al., 2012). When updrafts lead to cloud formation, Vilà-Guerau de Arellano et al. (2005) found a decrease of 10 to 50% of tracer mixing ratios averaged over the boundary-layer with respect to a situation without clouds due to the deepening of the boundary-layer. Clouds have multiple impacts on the atmospheric boundary layer as they induce a turbulent mixing of chemical compounds, which modifies the reaction rates. Then, they decrease the incoming solar radiation, which in turn disturb the photolysis reactions and alter the emissions of biogenic compounds, such as isoprene. Finally, they alter atmospheric chemistry due to soluble gas washout and chemical reactions occurring in cloud droplets.

Atmos. Chem. Phys. Discuss., https://doi.org/10.5194/acp-2017-969
Manuscript under review for journal Atmos. Chem. Phys.
Discussion started: 20 November 2017

Atmospheric Chemistry and Physics Discussions

High resolution simulations which explicitly resolve the turbulent and convective advection terms were conducted (Vilà-Guerau de Arellano and Cuijpers, 2000; Vilà-Guerau de Arellano et al., 2005; Kim et al., 2012, 2016) in order to asses the impacts of clouds and convective boundary layer on the mixing of chemical compounds. However, previous numerical studies on the impact of turbulent mixing of chemical compounds used mainly rather simple or little more detailed chemical schemes, resulting in possible limitations in the representation of the atmospheric chemistry.

The goal of this work is to evaluate the role of thermals on OH reactivity in the framework of a convective boundary layer with contrasted chemical environments in southern West Africa. This region is characterized by high occurrence of low-level stratus and stratus deck poorly represented in climate models, leading to errors in radiative forcing (Schrage et al., 2007; Knippertz et al., 2011; Schrage and Fink, 2012). Two chemical regimes represented by a detailed chemical scheme are contrasted in LES studies. The first simulation is influenced by biogenic emissions whereas the second one is characterized by anthropogenic emissions representative of Cotonou (Benin) in the center of the domain. The model experiments are presented in section 2. The section 3 present the dynamical and chemical results for the two cases and section 4 the discussion on these results.

2 Simulation description

2.1 Model configuration

LES simulations are performed with the mesoscale non-hydrostatic atmospheric model Meso-NH version 5.2.1 (http://mesonh.aero.obs-mip.fr/mesonh/), jointly developed by the Laboratoire d'Aérologie and the Centre National de le Recherche Météorologique (Lafore et al., 1998). Cloud microphysical processes are represented by the ICE3 scheme (Pinty and Jabouille, 1998) that includes six different types of hydrometeors. The turbulence is solved by a 3-dimensional scheme using a prognostic equation for the turbulent kinetic energy (Cuxart et al., 2000) with the turbulent mixing length given by the mesh size. Surface processes and interactions with the atmosphere are simulated by the SURFEx model (Masson et al., 2013) coupled with Meso-NH.

The resolution used is $50m * 50m$ for a domain size of 10 km $\times$ 10 km (200 $\times$ 200 grid points); the boundary conditions are cyclic. 10 km is the targeted mesh size of an increasing number of current large-scale chemistry models. Along the vertical, 121 levels are stretched from Δz = 20 m at the surface to 250 m on top of the domain at 20 km.

The simulation is run for three days whose two days consist in the spin-up for chemistry. Each day uses the same dynamical conditions and has the same initial and forcing thermodynamical fields. Results are shown only for the third day from 0600 to 1700 UTC, when the convective boundary-layer is well developed. A passive scalar is emitted only during this part of the simulation with a constant emission rate and is used to determine the boundary layer height (see section 2.4.1). Thermals are identified by the conditional sampling method implemented in the model by Couvreux et al. (2010), which relies on a radioactive-decay passive tracer mixing ratio and vertical velocity anomalies. This passive tracer is emitted starting from the beginning of the third day of simulation.

Initial and forcing dynamical fields come from Couvreux et al. (2014) who studied by means of a single column model the representation of the diurnal cycles of meteorological parameters in four observation sites in West Africa. Here we focus on the

"cloudy" regime of Couvreux et al. (2014), representative of the climate encountered close to the Guinean Gulf. The vegetation present in our simulation is dominated by tropical crops and open shrublands (35% of the domain for each type), sea (15%), inland water (5%), wetlands (5%) and tropical grasslands (5%) and a high moisture content is prescribed with a soil water index of 0.7 and 0.74 for the surface and the ground, respectively. Initial conditions and composite large-scale advections are extracted from ECMWF re-analysis (Agustí-Panareda et al., 2010) prepared for the AMMA campaign (Redelsperger et al., 2006). The present simulation is initialized at 0600 UTC with stable initial conditions, extracted from ECMWF AMMA reanalysis (black curve in Fig. 1b). The large-scale conditions from the ECMWF re-analysis also includes sea-breeze circulations from the surface to 500 m, linked to moist and cool advection throughout the simulation, topped by advection of dry and warm air from 1000 to 3000 m.

2.2 Chemical model setup

The applied chemical scheme ReLACS 3.0 (Reduced Lumped Atmospheric Chemical Scheme version 3.0) (Tulet et al., 2006), is a reduced version of the Caltech Atmospheric Chemistry Mechanism (CACM) (Griffin, 2002). This mechanism describes the reactions system of ozone gaseous precursors as well as of Secondary Organic Aerosol (SOA) with 365 reactions involving 87 species.

For both simulations, the initial vertical profiles of main primary chemical species are taken from airborne measurements made during the B235 flight of the AMMA campaign performed by the BAE-146 over a tropical forest (Table 1).

Biogenic emissions (Table 2) are taken from the MEGAN-MACC (Model of Emissions of Gases and Aerosols from Nature - Monitoring Atmospheric Composition and Climate) inventory (Sindelarova et al., 2014) except for NO. A maximum value of 10 ng.N.m^{-2}.s^{-1} is prescribed for nitrogen oxide emissions by soils in the simulation. Biogenic NO$_x$ emissions from GEIAv1 (Global Emission InitiAtive) inventory (Yienger and Levy, 1995) were proved to be too low for the studied region in comparison to estimations based on airborne measurements during the AMMA campaign (Stewart et al., 2008; Delon et al., 2010).

The emissions are constant in space and time except for NO, isoprene and monoterpenes, for which a gaussian diurnal cycle is used. For biogenic NO, the maximum emission is at 1300 UTC and the standard deviation of the gaussian curve is equal to 3 hours, these parameters are set in order to approximate the ground temperature as Mamtimin et al. (2016) and Yienger and Levy (1995) noted that NO emissions from soils are closely linked to soil temperature. For isoprene and sum of monoterpenes (represented as ISOP, BIOL and BIOH in the chemical scheme), the maximum is at 1200 UTC and the standard deviation is equal to 2.5 hours, chosen to fit the diurnal evolution of the solar radiation reaching the surface. This is in agreement with Guenther et al. (1991) who showed that isoprene emissions are thought to be very low when the Photosynthetically Active Radiation decreases. For isoprene and monoterpenes, the maximum emission values were defined to ensure that an equal amount of chemical species is emitted during one day compared to the constant value provided by MEGAN-MACC.

The anthropogenic emissions are provided by a squared patch in the center of the domain. Its area is chosen to be equal to half the domain area. However, the cyclic boundary conditions applied for these simulations tend to homogenize the chemical

Atmos. Chem. Phys. Discuss., https://doi.org/10.5194/acp-2017-969
Manuscript under review for journal Atmos. Chem. Phys.
Discussion started: 20 November 2017

mixing ratios. This affects especially long-lived species in the boundary layer and leads to the deletion of the biogenic emissions signature. Values of anthropogenic emissions are representative of Cotonou (Table 2) (Junker and Liousse, 2008).

In the following, the study focuses on isoprene for the biogenic case because it is the major biogenic VOC emitted to the atmosphere and influences the ozone and secondary organic aerosol formation (Guenther et al., 2006). For the anthropogenic case, a focus is made on the lumped C>2 aldehydes (ALD2 in the chemical scheme) because they have both primary and secondary sources and their role is very important in the troposphere as they contribute to the production of radicals and are precursors of ozone (Williams et al., 1996).

2.3 Metrics

In order to study the competition between chemical reactivity and turbulent mixing, as well as the inhomogeneity in chemical species mixing, Schumann (1989) introduced two dimensionless numbers, the Damkhöler number and the segregation coefficient. The first one corresponds to the ratio between the turbulence characteristic timescale τ_{turb} and the chemical reactivity timescale τ_{chem}. For a given compound A, the Damkhöler number D_a is :

$$D_a(A) = \frac{\tau_{turb}}{\tau_{chem}(A)} \text{ with } \tau_{turb} = \frac{w^*}{h} \text{ and } \tau_{chem}(A) = \frac{r_A}{\sum sinks(A)} \quad (1)$$

Where w^* and h refer to the convective velocity and the boundary-layer height, r_A is the mixing ratio of A and $\sum sinks(A)$ corresponds to the total chemical loss rate of A. Schumann (1989) used a threshold value of 0.1 for the Damkhöler number to distinguish slow (lower than 0.1) and fast (higher than 0.1) reactions. Later studies (Vilà-Guerau de Arellano and Cuijpers, 2000; Vilà-Guerau de Arellano et al., 2005; Molemaker and Vilà-Guerau de Arellano, 1998) used a threshold value of 1 to discriminate slow and fast chemical reactions and this method will be used in the following. If $D_a < 1$, the turbulent mixing is more efficient than the chemistry. If $D_a \simeq 1$, one can expect strong competition between dynamics and chemical reactivity. Finally, if $D_a > 1$, the chemical reactions occur faster than turbulent mixing. This turbulent mixing causes fluctuations of chemical specie mixing ratios in the LES domain, which can be quantified by the intensity of segregation. For a second order reaction implying two species A and B with a reaction constant $k : A + B \rightarrow C$, the intensity of segregation $I_S(A,B)$ is defined as :

$$I_S(A,B) = \frac{\overline{a'b'}}{\overline{a}.\overline{b}} \quad (2)$$

The lower case letters represent species mixing ratios at a grid point. The overbar denotes a spatial average, and the prime a deviation from this average. If $I_S(A,B) = -1$, then the two species are completely segregated and no reaction will take place between them. If $I_S(A,B) = 0$, compounds are perfectly mixed. A positive segregation coefficient means that covariance between species is similar and thus the mean chemical reaction rate would be higher in comparison to a perfect mixing. The segregation is calculated with mixing ratios anomalies related to spatial averages in numerical models. Ouwersloot et al. (2011) stated that these averages should correspond to the complete mixing volume in order to allow comparisons between models

Atmos. Chem. Phys. Discuss., https://doi.org/10.5194/acp-2017-969
Manuscript under review for journal Atmos. Chem. Phys.
Discussion started: 20 November 2017

Atmospheric Chemistry and Physics Discussions

and measurements. In the following, the large-scale spatial average is calculated over the 10 km x 10 km model domain. One can define an effective average reaction rate $\overline{R}$ that includes the turbulent mixing impact on the chemical reactivity as :

$$R_e = k_e \cdot \overline{a} \cdot \overline{b} \text{ with } k_e = k \cdot (1 + I_S(A,B)) \tag{3}$$

Here, k_e is the effective mean reaction constant and bars over species denote averages over the domain.

In the current LES experiments, chemical reaction rates are calculated with a focus on OH. The OH radical reactivity R_{OH} corresponds to the inverse of OH lifetime τ_{OH} and is defined as :

$$R_{OH} = \frac{1}{\tau_{OH}} = \sum_i^n k_{(\chi_i + OH)} \cdot \chi_i \tag{4}$$

In Equation 4, $k_{(\chi_i+OH)}$ represents the reaction constant between OH and the i-th reactant, and χ_i corresponds to its concentration. In a similar way than the effective reaction constant R_e, an effective reactivity for the OH radical R^e_{OH} is defined by including the effect of turbulent mixing in Equation 4 as :

$$R^e_{OH} = \sum_i^n k^e_{(\chi_i+OH)} \cdot \chi_i \tag{5}$$

$$= \sum_i^n k_{(\chi_i+OH)} \cdot (1 + I_S(OH, \chi_i)) \cdot \chi_i \tag{6}$$

$$R^e_{OH} = R_{OH} + \sum_i^n k_{(\chi_i+OH)} \cdot I_S(OH, \chi_i) \cdot \chi_i \tag{7}$$

R_{OH} denotes the OH total reactivity calculated with averaged values. In order to obtain the relative deviation of the total OH reactivity from the reactivity computed with averaged mixing ratios, a factorization is performed on Equation 7, which results in :

$$R^e_{OH} = R_{OH} . (1 + \frac{\sum_i^n k_{(\chi_i+OH)} \cdot I_S(OH, \chi_i) \cdot \chi_i}{R_{OH}}) \tag{8}$$

From Equation 8 the mean relative error, $E_{k_{OH}}$, made on the total OH reactivity only considering averaged values is :

$$E_{R_{OH}} = \frac{\sum_i^n k_{(\chi_i+OH)} \cdot I_S(OH, \chi_i) \cdot \chi_i}{R_{OH}} \tag{9}$$

The segregation intensity used to compute the mean error corresponds to deviation from boundary layer averaged values. This error is not considered in previous numerical studies looking at the identification of the missing part of OH reactivity.

Atmos. Chem. Phys. Discuss., https://doi.org/10.5194/acp-2017-969
Manuscript under review for journal Atmos. Chem. Phys.
Discussion started: 20 November 2017

Atmospheric Chemistry and Physics Discussions

Indeed, using a box model or a single column model like Mogensen et al. (2011); Whalley et al. (2011, 2016) could lead to neglecting the turbulent motions that could affect the redistribution of chemical species within the atmospheric boundary layer.

2.4 Simulation assessment

2.4.1 Dynamics

The diurnal evolution of the boundary-layer height (BLH) is analyzed in Fig. 1a. It is diagnosed from two different methods. The first one corresponds to a determination according to the bulk Richardson number method as presented in Zhang et al. (2014). The boundary layer height is defined as a threshold value for the bulk Richardson number Ri_b, which is computed at a given height with the virtual potential temperature θ_v and horizontal wind speeds u_z and v_z at this altitude and at the surface :

$$Ri_b = \frac{(g/\theta_{v0})(\theta_{vz} - \theta_{v0})z}{u_z^2 + v_z^2} \tag{10}$$

A clear diurnal cycle is observed, the maximum height being at 1400 UTC and the minimum during nighttime (Fig. 1a, red line). Daytime BLH is consistent with observations from Cotonou in West Africa studied by Gounou et al. (2012) who noticed daily variabilities ranging from 400 to 600 m. In this work the boundary-layer height is derived from radiosoundings by comparing the virtual potential temperature at one level and the averaged value below. The LES Meso-NH model fails to reproduce the observed shallow nocturnal BL of about 100 m deep during the AMMA campaign. Couvreux et al. (2014) explained the very low nighttime BL by the strong stratification in the model. This first diagnostic does not include the cloud layer on the boundary layer.

The second method determines the boundary layer height according to Vilà-Guerau de Arellano et al. (2005) by identifying the height at which a passive bottom-up scalar emitted the third day is equal to 0.5% of its surface value. Kim et al. (2012) mentioned that this definition could be valuable when studying the boundary layer deepening due to clouds. This diagnostic captures the growth of the boundary layer height due to the development of cumulus clouds (Fig. 1a, blue line) and is used to mark the BL height in the following.

The range of simulated virtual potential temperature (Fig. 1b) slightly overestimates the AMMA observations in Cotonou of Gounou et al. (2012) in the lowest 500m as shown by Couvreux et al. (2014). Both the dry and cloudy layers are identified by two inflections on the vertical profiles of virtual potential temperature (Fig. 1b). The first inflection increases from 400 m at 0600 UTC to 600 m at 1700 UTC corresponds to a thin inversion zone between the well-mixed dry layer and the cloudy layer above it. The second inflection defines the top of the boundary layer ranging from 500 m at 0600 UTC to 1600 m at 1700 UTC.

Cloud cover over West Africa is an important feature of the African monsoon but is poorly represented by global models (Hannak et al., 2017). This could lead to too low simulated clouds and too high incoming radiation at the surface that imply too high diurnal cycles of temperature and relative humidity over this region. The nocturnal low-level stratus have been studied during the monsoon period at Parakou (Benin) by Schrage et al. (2007) with radiosondes. The authors found that turbulent processes are responsible for cloudy nights whereas clear nights are associated with a nocturnal inversion promoting the decoupling of surface and lower atmosphere. Schrage and Fink (2012) investigated the nighttime cloud formation. They stated

that the presence of a nighttime low-level jet induces a shear-driven vertical mixing of moisture accumulated near the surface. This leads to cloud formation whose cover is likely to persist until the early afternoon (Schrage et al., 2007; Schrage and Fink, 2012). This feature is simulated in this work as low level stratus clouds occupy a large fraction of the simulated domain in the morning (Fig. 1a and 2a;2c). In the afternoon, the cloud deck breaks up and less uniform but higher cumulus clouds are simulated (Fig. 1a, 2c and d).

Throughout the growth of the boundary layer, dry thermals develop capped by the temperature inversion zone. Some thermals penetrate this inversion (Fig. 2) and cloud formation occur at the upper part of the updrafts. The vertical profiles of the fraction area (Fig. 3) occupied by thermals exhibit a local maximum at the height corresponding to the separation between the two layers. This altitude is variable through the simulation but tends to stabilize between 500 and 600m in the early afternoon and is associated to a favored detrainment zone. The peaks observed at the surface and at the top of the cloudy layer correspond to two others local maxima. Due to the deepening of the boundary-layer, the top of the cloudy layer is increasing throughout the simulation (Fig. 2,3). Simulated convective velocity w^* (resp. turbulence characteristic timescale τ_{turb}) ranges from $1cm.s^{-1}$ (resp. $6h$) in the morning to $1m.s^{-1}$ (resp. 20 min) at midday.

2.4.2 Atmospheric chemistry

Typical diurnal cycles are obtained for isoprene in the biogenic case and for OH in the biogenic and anthropogenic cases, where both compounds exhibit maximum mixing ratios around midday (Fig. 4). For the biogenic case, the simulated isoprene mixing ratios averaged from the surface to 600 m reach a maximum close to 1 ppbv (Fig. 4a) at noon, when isoprene emissions are the highest. It is on the same range as AMMA measurement studied by Saxton et al. (2007) who found a maximum of 1.5 ppbv on the composite diurnal cycle of isoprene at midday. In our study, the ozone mixing ratios do not exhibit strong variability throughout the day. The simulated values around 18 ppbv are lower than observations collected over forested areas (Table 3) ranging from 22 to 30 ppbv. NO_x mixing ratios are close to 0.2 ppbv on average around midday (Fig. 4b) and are in agreement with AMMA measurements where a mean value of 0.1 ppbv of NO_x has been observed. Simulated OH mixing ratios vary between 0 and 0.18 pptv (Fig. 4a), within the observational range of 0.05 to 0.15 pptv during the AMMA campaign (Table 3). The biogenic environment is characteristic of a NO_x limited regime.

The chemical regime induced by the anthropogenic emissions is contrasted with the previous biogenic case (Fig. 4c,d), including NO_x emissions nearly forty times higher at 1300 UTC. Averaged NO_x mixing ratio is 1.5 ppbv at midday (Fig. 4d), which is similar to the averaged value of 1 ppbv measured during a flight over Cotonou during the AMMA campaign (Table 3). The increase in NO and NO_2 leads to important oxidant formations. OH mixing ratios vary between 0 and 0.40 pptv in the simulation, in agreement with AMMA measurements ranging from 0 to 0.50 pptv over Lagos (Table 3). Ozone is produced throughout the simulation but does not exhibit strong spatial variabilities. Its mixing ratios vary from 17 ppbv in the morning to 82 ppbv in late afternoon. This is higher than observations collected over several cities in West Africa varying between 26 and 40 ppbv (Table 3). ALD2 is continuously increasing during this case through chemical production and emissions (Table 2). Its mixing ratios range from less than 1 ppbv in the morning to 11 ppbv at the end of the simulation. Unfortunately, no C>2

Atmos. Chem. Phys. Discuss., https://doi.org/10.5194/acp-2017-969
Manuscript under review for journal Atmos. Chem. Phys.
Discussion started: 20 November 2017

aldehydes observations, except formaldehyde, were available from the AMMA experiment despite the use of a PTR-MS due to interferences during the measurements for m/z=45 identified as acetaldehyde (Murphy et al., 2010).

A minimum of NO is found around 1200 UTC for both cases. At that time, NO is efficiently converted into NO_2. However, NO_2 chemical transformations in reservoir species such as peroxy pentionyl nitrate (PAN1 in the chemical scheme), peroxy acetyl nitrate (PAN2) or HNO4 are net sinks for NO_2. The chemical balance between reservoir species and NO_2 represent 2.12% of the net destruction of NO_2 averaged over the domain at 20 m and 1200 UTC for the biogenic case, and 34.2% for the anthropogenic case. As a consequence, less NO_2 is available to convert into NO, which explain the midday low NO mixing ratios (Fig. 4b and d).

3 Vertical transport and chemical reactions in the convective boundary layer

3.1 Impact of turbulent mixing on the OH reactions

3.1.1 Vertical transport and Damkhöler numbers

Isoprene is highly reactive, especially towards OH, and is rapidly consumed in the boundary layer linked to its chemical lifetime τ_{ch} approximately equal to 30 mn in the biogenic case. The Damkhöler number of isoprene is close to 1 (Table 4), indicating that the isoprene chemical lifetime is comparable with the timescale of turbulent mixing. This implies that chemical reactions and turbulent mixing are competing processes for this compound. Isoprene is both transported and consumed inside the thermals and exhibit vertical and horizontal gradients (Fig. 5a). Average profiles of isoprene are decreasing with altitude (Fig. 5a). The lower mixing ratios on the dashed line, denoting updrafts-free region, are close to the domain averaged values due to the domain coverage by thermals (Fig. 3). Updrafts regions contain isoprene higher mixing ratios and anomalies are consequent over the whole boundary layer.

For the biogenic case, OH has a very short chemical lifetime of the order of 0.2 s. The OH radical reaches rapidly a chemical equilibrium and is nearly undisturbed by the turbulent mixing as shown by its large Damkhöler number (Table 4). As a consequence, OH mixing ratios (Fig. 5b) has nearly homogeneous values below 600 m with no distinction between thermals and their environment. Average profiles of OH (Fig. 5b) shows no strong variability below 600 m in the boundary layer. Above this height, thermals are less concentrated in OH on average but differences are relatively low. Since OH is almost constant over the boundary layer, the highest reaction rate for the oxidation of isoprene by OH ($k_{OH+ISOP}\,[ISOP]\,[OH]$) is located where isoprene mixing ratios are the highest. This implies that both the surface and air lifted by thermals are preferential reaction zones in the boundary layer.

For the anthropogenic simulation, ALD2 reaction rate with OH is lower than isoprene. Its calculated Damkhöler number (≈ 0.17) indicates that turbulent mixing dominates over chemical reactions (Table 4). Consequently, ALD2 is efficiently transported by updrafts (Fig. 5c). The contrast between concentrated air parcels lifted up by thermals and relatively diluted air outside is illustrated by the large differences in the ALD2 average profile in thermals and in the environment (Fig. 5c). Sim-

Atmos. Chem. Phys. Discuss., https://doi.org/10.5194/acp-2017-969
Manuscript under review for journal Atmos. Chem. Phys.
Discussion started: 20 November 2017

ilarly to isoprene in the biogenic case, two local maxima are present 600 and 1100m, representing the two-layer structure presented above.

OH mixing ratios are nearly twice higher in the anthropogenic environment than the biogenic case. That induces a more reactive atmosphere and a lower chemical lifetime for species whose OH is the main sink in the boundary layer. OH has a very low chemical lifetime of 0.07s in this simulation, which represents a large Damkhöler number close to 12 000. OH mixing ratios are maximum in thermals (Fig. 5d) due to the transport of OH precursors, such as NO_x, and fast chemical equilibrium. Conversely, lower mixing ratios on OH average profiles (Fig. 5d) corresponds to regions without updrafts, leading to strong OH anomalies inside updrafts.

3.1.2 Vertical profile of segregation intensity

Negative values of segregation coefficient up to -30% are calculated at the top of the cloudy boundary layer from 1000 to 1700 UTC which means that OH and isoprene are partly segregated in this frontier zone. In other words, a well mixed atmosphere hypothesis would conduct to a 30% overestimation of the reaction rate at the frontier between the boundary layer and the free troposphere. The negative segregation means covariances of isoprene and OH are of opposite signs (Eq. 2). This is due to lower OH mixing ratios in thermals than the environment. These results are consistent with the previous studies of Li et al. (2016); Kim et al. (2016); Ouwersloot et al. (2011) (see Discussion).

In the biogenic case, isoprene anomalies in thermals are important from the surface (+0.48 ppbv on average at midday) to the top of the boundary layer (+0.1 ppbv on average at midday) and are thought to be always positive as it is uniformly emitted at the ground (Fig. 5a). On the opposite, OH mixing ratios are almost constant in the boundary layer at 1200 UTC (Fig. 5b), so the magnitude of its anomalies are expected to be low. Besides, its very short chemical lifetime induces that OH is quickly in equilibrium with its surroundings, which implies that its fluctuations are mostly due to thermals transporting air originating from a different chemical environment. Thus, isoprene anomalies are thought to be the major driver in segregation magnitude over the boundary layer whereas OH anomalies are related to the segregation sign.

Positive values around +5% are calculated at 700 meters starting from 1400 to 1800 UTC (Fig. 6a). The segregation intensity become positive due to positive anomalies of both compounds. Due to the decreasing isoprene emissions in the afternoon, OH destruction slows down, especially inside thermals. They are still active to transport enough NO to react with HO_2 to produce OH, which induces higher OH mixing ratios inside updrafts.

Before 0900 UTC near the surface, the segregation coefficient in the anthropogenic simulation between OH and ALD2 is negative up to -8% in the lower 200m (Fig. 6b), due to the anthropogenic emission patch. Simultaneously, positive segregations develop at the top of the boundary layer from 0700 UTC to 1230 UTC with a maximum of 16% at 1000 UTC and from 1530 to 1730 UTC. The positive segregation is related to the concomitant transport of ALD2 and precursors of OH by thermals. ALD2 is emitted at the surface, thus its anomalies are high and positive inside updrafts. As an example, at midday, anomalies are +0.5 ppbv on average at the surface and nearly +4 ppbv at the top of the boundary layer. However, in this case, OH anomalies are more difficult to predict. Except for positive segregation simulated between 500 and 1400 m from 1130 to 1600 UTC with values ranging from 2 to 4%, ALD2 and OH can be considered well mixed in the central part of the boundary layer. The ALD2

Atmos. Chem. Phys. Discuss., https://doi.org/10.5194/acp-2017-969
Manuscript under review for journal Atmos. Chem. Phys.
Discussion started: 20 November 2017

oxidation reaction by OH is accelerated up to 16% at the top of the cloudy layer from the morning to the early afternoon compared to a perfect mixing assumption.

Regarding the two simulations, the segregation has both spatial and temporal variations. The maximum values of segregation coefficient are calculated near the top of boundary layer. Below and during daytime, considered species are well mixed for both cases. It means that the highest decrease (resp. increase) induced by thermals of isoprene (resp. ALD2) + OH reaction is located near the boundary layer top.

3.2 OH budget and reactivity in a convective boundary layer

The precedent part emphasizes the non uniform mixing between isoprene and OH for the biogenic case and between OH and ALD2 for the urban case, and the implication for the reaction between these species. However, this feature has to be accounted for every OH reactants in order to have the full picture of the total OH reactivity and understand how the Meso-NH model compute the OH budget in different chemical regimes.

3.2.1 OH budget in thermals versus environment

In order to identify and quantify the major OH sources and sinks in the boundary layer, the instantaneous chemical budget of OH at 20 meters above ground level is investigated at 1200 UTC for both environments (Fig. 7). This height is the first model level and allows a comparison between the results from the simulations and from measurements in the literature. The budget distinguishes between updrafts and updrafts-free columns. Percentages are related to the fraction of the overall production and destruction in or outside thermals. In the biogenic case (Fig. 7a), the OH budget is dominated by its destruction by isoprene oxidation (41.7 % of the total loss in updrafts and 29.3 % of the total loss in the rest of the domain) and its production by peroxy radicals reaction with HO_2 (37.2 % of its total source in updrafts and 42.4 % of the total source in non updrafts) and NO reaction with HO_2 (32.4 % of the total source in updrafts and 17.8 % of its total source in the rest of the domain). In that case, the peroxy radicals are mainly formed by the oxidation of isoprene and its degradation products. The absolute value of OH reactivity is higher in thermals than in the rest of the domain.

The OH budget for the anthropogenic case (Fig. 7b) shows that the chemical reactivity is higher inside thermals at the surface compared to the rest of the domain. The budget is largely dominated by the production of OH by NO+HO_2 and by O^1D+H_2O. Over the whole domain, ALD2+OH is the most important sink at the surface or at 500 m, followed closely by the oxidation of carbon monoxide.

Similar results are obtained at 500 m (not shown) that confirm the higher chemical reactivity inside thermals compared to their environment.

3.2.2 OH reactivity in the convective boundary layer

The OH reactivity for the biogenic case (Eq. 4) at 20 m is maximum around midday and is equal to 6.0 s^{-1}, 4.25 s^{-1} and 4.55 s^{-1} respectively in updrafts, non-updrafts and averaged over the domain (Fig. 8a). This feature is linked to the photochemistry

maximum activity at noon, and the diurnal cycle of emissions amplifies this phenomenon. At that time and near the surface, many chemical compounds are available to react with OH, which leads to a high value of reactivity. The values in updrafts are higher than outside due to higher reactants mixing ratios inside thermals (Fig. 5a). The arithmetic difference between updrafts and non-updrafts is maximum at 1200 UTC and is about 1.75 s^{-1}. As the thermals occupy less than 15% of the domain (Fig. 3), the evolution of the domain-averaged OH reactivity is very similar to these related to updrafts-free region.

The diurnal cycle of OH total reactivity with a maximum around midday in a biogenic environment is well documented in literature from observations of OH reactivity for a Mediterranean forest (Zannoni et al., 2016), for temperate forests (Sinha et al., 2008; Ramasamy et al., 2016) but also for tropical forests (Nölscher et al., 2016; Williams et al., 2016). The values of OH reactivity in or outside thermals in the present study are the lower bound of measurements over forests and gathered in Yang et al. (2016), between 1 and 76 s^{-1}.

The mean relative error made on OH reactivity is calculated following Equation 9 (not shown). It is generally negative throughout the simulation, increases during the morning and is maximum in the early afternoon with a peak at -9% at 1430 UTC. In other words, neglecting the segregation of reactive species turbulent mixing in the boundary layer would overestimate the OH reactivity by 9% at the maximum in an environment dominated by biogenic emissions.

For the anthropogenic case, the total OH reactivity (Eq. 4) in thermals or in the rest of the domain does not display a clear diurnal cycle (Fig. 8b). From the 0800 UTC value of 11.6 s^{-1}, the domain-averaged OH reactivity fluctuates but tends to increase to 14.2 s^{-1} at 1600 UTC. The evolution of the OH reactivity in thermals is similar and ranges from 14.8 s^{-1} at 0800 UTC to 17.7 s^{-1} at 1600 UTC. For the same period, the values in updrafts-free domain vary between 11 and 13.5 s^{-1}.

As a consequence of the increased OH reactants mixing ratios in the boundary layer (Fig. 4c and d), OH reactivity is higher in this case compared to the biogenic simulation. The mean relative error of the OH reactivity (Eq. 9) is generally positive throughout the simulation (not shown). It ranges between 0 to 4% from 0900 to 1730 UTC with a maximum value of 6% at 1800 UTC. In that case, the turbulent mixing induces a moderate increase up to 6% of the total OH reactivity for two reasons. The segregation effect is limited to the last 200 m of the boundary layer. Thus averaging on the whole boundary layer suppress the extreme values. Moreover, some chemicals could have negative segregation towards OH that may compensate the positive values simulated for ALD2 and OH (Fig. 6b).

4 Discussion

The redistribution of chemical species in the boundary layer induces a different mean reaction rate between compounds when compared to a situation where chemical species would be perfectly mixed. This assumption used in regional or large scale atmospheric models leads to errors on chemical reactivity as the turbulent mixing occurs at scales smaller than the grid length (Vinuesa and Vilà-Guerau de Arellano, 2005).

In a biogenic environment characterized by low NO_x conditions, Kim et al. (2016) found negative segregation between isoprene and OH varying between -3% near the surface to -10% in the cloud layer due to increasing OH mixing ratios in thermals with altitude. That implied positive isoprene anomalies and negative for OH in the frontier region between the boundary layer

Atmos. Chem. Phys. Discuss., https://doi.org/10.5194/acp-2017-969
Manuscript under review for journal Atmos. Chem. Phys.
Discussion started: 20 November 2017

and the free troposphere, these features are reproduced in our biogenic simulation even though our values of segregation are higher in the cloud layer (Fig. 6).

Using a simple chemistry, Ouwersloot et al. (2011) found an almost constant value of -7% for the segregation between OH and isoprene over the amazonian forest in the boundary layer. It was the results of positive isoprene anomalies due to transport by thermals and negative OH anomalies due to consumption therein. Negative segregation ranging from -2% to -5% inside the convective boundary layer have been simulated by Li et al. (2016) and Kim et al. (2016). In the biogenic case of our work, negative segregation of few percent in the middle of the boundary layer is reproduced. The discrepancies between this last simulation and the previous cited studies are partly due to differences between the convective boundary layer dynamics, resulting in different characteristics of turbulent structure. Moreover, using simple chemistry rather than a comprehensive chemical mechanism could lead to an insufficient representation of the OH chemistry. This results in neglecting some OH destruction reactions and eventually some OH recycling pathways. Besides, Ouwersloot et al. (2011) and Kim et al. (2016) investigated the sensitivity of segregation to NO_x. It was found that different NO_x levels imply discrepancies in the segregation of OH and other compounds as they contribute to the OH production.

The segregations between isoprene and OH inferred from observations are higher than numerical studies calculated. Butler et al. (2008) found a segregation close to -13% over a forest in Suriname and Dlugi et al. (2010) calculated over a deciduous forest a reduction of 15% in the effective reaction rate between OH and isoprene at the surface due to incomplete mixing. This is higher than the segregation computed at the surface in the biogenic case of the present study but when considering the complete mixing volume, the segregation computed with boundary layer averaged mixing ratios is negative and its maximum value is -16% at 1300 UTC.

Kim et al. (2012) studied by means of a LES the OH budget in a biogenic environment averaged over the domain and over time from 1330 to 1430 LT with a chemical scheme adapted from MOZART v2.2. They found, for a low NO_x case with ozone mixing ratios close to 64 ppbv, that the OH production was mostly influenced by four predominant reactions (including O^1D + H_2O, HO_2 + O_3, H_2O_2 photolysis and HO_2 + NO). They found that the OH loss by reaction with isoprene was dominant near the surface, followed by the reactions with CO and formaldehyde. The OH reactivity contribution of the BVOC species was simulated by Li et al. (2016) for three distinct biogenic cases of the DISCOVER-AQ (Deriving Information on Surface Conditions from Column and Vertically Resolved Observations Relevant to Air Quality) campaign. Isoprene was a dominant sink for OH, about 25-30% of the OH reactivity was linked to BVOC reactions at 0.3 km during midday. The contribution of formaldehyde was comparable to isoprene at that height, with HCHO mixing ratios ranging from 2 to 4.5 ppbv at the surface.

Yang et al. (2016) found that in forest areas the OH budget was largely dominated by isoprene and its oxidation products. As an example, over a Mediterranean forest, Zannoni et al. (2016) measured the OH reactivity, as well as the concentration of biogenic compounds. They found that isoprene was the dominant sink for OH and contributes up to 74% of OH total reactivity during daytime due to its high reactivity towards OH and its high concentration over the forested area. The isoprene predominance in OH loss is reproduced in the OH budget of the biogenic environment of the present study, as well as for carbon monoxide. Formaldehyde mixing ratios are close to 2 ppbv, which explains that this is not a important sink as isoprene, but remains not negligible in the OH loss. The OH production in the biogenic case is similar to Kim et al. (2012) as almost the

Atmos. Chem. Phys. Discuss., https://doi.org/10.5194/acp-2017-969
Manuscript under review for journal Atmos. Chem. Phys.
Discussion started: 20 November 2017

Atmospheric Chemistry and Physics Discussions

same production terms are present. However, the overall production is dominated by peroxy radicals reaction with HO_2 and the ozone mixing ratios of 18 ppbv decrease the importance of O^1D + H_2O source for OH.

However, the mechanism used to represent atmospheric chemistry in our simulation has a fast OH cycling through the reaction of peroxy radicals RO_2 with HO_2. An uncertainty comes from this reaction yield that is higher than laboratory studies (Hasson et al., 2004; Jenkin et al., 2007; Groß et al., 2014; Winiberg et al., 2016). This imply an overestimation of OH mixing ratios, especially in the biogenic case where RO_2 are important. As the hydroxyl radical is recycled through the isoprene oxidation products, it tends to reduce the impact of isoprene chemistry on OH mixing ratios and thus influence the low segregation simulated in the core of the boundary layer. This is similar to a case considered by Stone et al. (2011) where a recycling mechanism ISOPO2 + HO_2 → ISOPOOH + 3 OH have been proposed to increase the simulated OH concentrations. This reaction imply that isoprene have no net impact on OH concentrations. This conclusion is drawn also by Kubistin et al. (2010) who found better agreement between simulated and measured HO_x concentrations by ignoring the isoprene chemistry. As the chemistry of isoprene is not well understood, the results obtained in our work are subject to these uncertainties.

Aldehydes have not been considered in previous works studying segregation. Auger and Legras (2007) calculated the segregation at 250 m and 1100 UTC between each species of the chemical model CHIMERE used in their simulation. They found a segregation ranging from 0 to -1% between OH and acetaldehyde. This is comparable to range of results of the anthropogenic case of the present study (Fig. 6b) considering the incomplete mixing between OH and C>2 aldehydes at the same height. The segregation computed relatively to boundary layer averaged values is very similar to the mean relative error (Eq. 9) made on the OH reactivity due to the strong predominance of ALD2 in the OH budget. It is generally negative throughout the simulation and varies from -0.02 at 0700 UTC to -0.015 at 1730 UTC. As pointed out by the vertical profiles of segregation (Fig. 6b), the impact of turbulent mixing on the chemical reactivity depends on the considered time of the day. In this case, a reduction of few percents of the reaction rate of ALD2+OH is found in the early morning and the late afternoon, and an increase up to 4% is simulated between 0800 and 1600 UTC over the whole boundary layer. This reveals a small impact of turbulent mixing on the chemical reactivity.

Several instrumental studies looked at the OH total reactivity in urban environments, and especially at the OH budget. Hansen et al. (2015a) found in an urban environment that NO_x contribution (50 to 55%) was the most important to the OH loss ranging considering NO_x mixing ratios between 10 and 300 ppbv. The next most important contribution came from the OVOCs (especially aldehydes and ketones) that varied from 15 to 25% of the OH destruction with mixing ratios close to 20 ppbv. Some discrepancies exist between this experimental study and the OH budget for the anthropogenic case in our study (Fig. 7b). Given the NO_x mixing ratios simulated in the present study (< 3 ppbv at midday), they are not an important sink for OH as measured by Hansen et al. (2015a). However, the range of OVOCs contribution reported by Hansen et al. (2015a) is comparable to what is found for ALD2 in the anthropogenic case.

In the city of Tokyo, Sadanaga et al. (2004) found that the OH budget was dominated by NMHCs and by OVOCs. In their study, the OVOC category grouping acetaldehyde, formaldehyde, methanol, ethanol and acetone, can contribute up to 18% of the OH reactivity. If aggregated, the species constituting the NMHCs category are the predominant sink for OH in our anthropogenic simulation, as observed by Sadanaga et al. (2004). However, C>2 aldehydes have higher contribution in the OH

destruction in our study than in Sadanaga et al. (2004). It could be a consequence of the cyclic boundary conditions prescribed at the borders of our domain, which can cause the ageing of air masses and increase mixing ratios of secondary products such as aldehydes.

Lelieveld et al. (2016) studied the global distribution and budget of OH radical using the model EMAC (ECHAM/Messy Atmospheric Chemistry) coupled with the the Mainz Organics Chemistry (MOM). They found that the annual mean OH reactivity near the surface ranged from 10 to 20 s^{-1} in southern West Africa, which is in agreement with the results of the anthropogenic case but slightly higher than values obtained in our biogenic case. However, Nölscher et al. (2016) studied, by means of observations, the seasonality in rainforest air reactivity and noticed that the total OH reactivity was much lower during the wet season than during the dry season due to a lowering in temperature and incoming radiation. More precisely, measurements of reactivity made during the wet season varied between 6 and 12 s^{-1} with an average value of 9.9±5.2 s^{-1} at 24 meters, which is much closer to the Meso-NH model results. Moreover, the estimations of Nölscher et al. (2016) OH reactivity missing fraction, between 5 and 15 %, are of the order of the overestimation of the total OH reactivity neglecting the turbulent mixing over a rainforest in a convective boundary layer (Fig. 8a).

Aqueous-phase chemistry was not considered here, nor the exchanges between gas and aqueous phases. However, it could have an impact on soluble species mixing ratios, such as formaldehyde and H_2O_2 through the capture and degassing cycles of these compounds. Lelieveld and Crutzen (1990) showed a decrease in oxidative capacity of the atmosphere through aqueous-phase reactions via a significant decrease in ozone mixing ratios, but also HO, formaldehyde and nitrogen oxides. However, variables effects of aqueous-phase chemistry on gas-phase compounds concentrations exist (Barth et al., 2003) and OH concentrations could decrease in clouds (Mauldin et al., 1997), reducing the cleansing capacity of the atmosphere and potentially increasing the segregation between OH and its reactants.

5 Conclusions

A numerical simulation coupled with a realistic chemical mechanism is performed with the atmospheric model Meso-NH to study the impact of thermals on the oxidizing capacity of the atmosphere. The fine grid resolution of the LES version of the model allows the thermals to be explicitly resolved spatially and temporally. Identification of thermals was based on a conditional sampling method relying on a radioactive-decay passive scalar. The study of impact of turbulent mixing on the chemical species redistribution, but also the consequences on the OH reactivity, is performed in a natural environment and a more contrasted urban case.

The differentiated transport by thermals is dependent of the chemical lifetime of compounds, which is represented by the Damkhöler number. This transport induces heterogeneities in the species repartition within the boundary layer, but also has an impact on the mean chemical rate between reactive species. Between isoprene and the OH radical, a 30% affective decrease of the reaction rate is calculated at the top of the boundary layer in a biogenic environment compared to a perfectly mixed case. In the urban case, the reduction of the mean chemical rate between the OH radical and C>2 aldehydes can reach 8% at the

surface in the early morning while this reaction is increased up to 16% at the top of the boundary layer during most part of the simulation.

Thermals transporting species emitted at the surface can lead to different chemical regimes inside updrafts and the environment. For both cases, the surface and the transported parcel correspond to preferential reaction zones, where the reactivity is the highest. This is especially the case for the OH radical whose precursors are either transported by thermals or created inside. For the natural case, the major OH precursors close to the surface are radicals originating from the oxidation of isoprene and its degradation products whereas O^1D+H_2O reaction become more predominant with increasing altitudes. In the urban case, OH is mainly produced through the reaction between HO_2 and NO, at the surface or higher in the boundary layer. This leads to a higher oxidation capacity in air transported by thermals for both cases. The heterogeneity in OH reactivity within the boundary layer have repercussions on the mean OH reactivity. In order to evaluate this impact, the mean relative error is introduced and includes the effect of turbulence on the mean effective reaction rate between OH and its reactants. A maximum overestimation close to 9% of the total OH reactivity in the biogenic case is found compared to a reactivity that would be calculated with boundary layer averaged values. This is in the range of OH reactivity missing fraction, from 5 to 15%, found by Nölscher et al. (2016) during the wet season at midday over the amazonian forest but lower than Lelieveld et al. (2016). The segregation cannot fully reconcile the OH concentration measurements and simulations, but it remains an interesting candidate to consider while studying the total OH reactivity over a tropical forest during the wet season. In the urban environment, the mean relative error is not constant over time but fluctuates between an overestimation of 5% and an underestimation of 6%.

This study addresses the impact of moist thermals on the oxidative capacity of the atmosphere on two contrasted chemical situations in a wet environment represented by the monsoon flow. However, Nölscher et al. (2016) noticed a consequent seasonal cycle in the OH reactivity over an amazonian forest ranging from 10 s s^{-1} in the wet season to 62 s^{-1} in the dry season. It could be interesting to assess the impact of turbulent mixing on chemistry in the dry season over the southern part of West Africa. Moreover, the influence of urban area in this study was only linked to chemical emissions. This work should be repeated by taking into account the dynamical forcing due to the presence of the urban area in the same way that Ouwersloot et al. (2011) introduced heterogeneous surface conditions over forest and savannah patches. These authors showed that the difference in buoyancy fluxes at the surface could have an impact on the redistribution of species, and thus on the segregation. Finally, the presence or clouds was only considered from a dynamical view. Adding the aqueous phase chemistry in those simulations could provide a further insight into the impact of moist thermals on the chemical reactivity.

Acknowledgements. The authors are very grateful to Mat Evans for his helpful comments and discussions. The research leading to these results has received funding from the European Union 7th Framework Programme (FP7/2007-2013) under Grant Agreement no.603502 (EU project DACCIWA: Dynamics-aerosol-chemistry-cloud interactions in West Africa). This work was performed using HPC resources from GENCI-CINES (Grant 2016-A0010100005). The authors acknowledge ECCAD (http://eccad.aeris-data.fr/) for the archiving and distribution of emissions data.

References

Agustí-Panareda, A., Beljaars, A., Ahlgrimm, M., Balsamo, G., Bock, O., Forbes, R., Ghelli, A., Guichard, F., Köhler, M., Meynadier, R., and Morcrette, J.-J.: The ECMWF re-analysis for the AMMA observational campaign, Quarterly Journal of the Royal Meteorological Society, 136, 1457–1472, https://doi.org/10.1002/qj.662, http://doi.wiley.com/10.1002/qj.662, 2010.

Ancellet, G., Leclair de Bellevue, J., Mari, C., Nedelec, P., Kukui, A., Borbon, A., and Perros, P.: Effects of regional-scale and convective transports on tropospheric ozone chemistry revealed by aircraft observations during the wet season of the AMMA campaign, Atmos. Chem. Phys, 9, 383–411, https://hal-univ-diderot.archives-ouvertes.fr/hal-00355175/document, 2009.

Auger, L. and Legras, B.: Chemical segregation by heterogeneous emissions, Atmospheric Environment, 41, 2303–2318, https://doi.org/10.1016/j.atmosenv.2006.11.032, http://linkinghub.elsevier.com/retrieve/pii/S1352231006011319, 2007.

Barth, M. C., Sillman, S., Hudman, R., Jacobson, M. Z., Kim, C.-H., Monod, A., and Liang, J.: Summary of the cloud chemistry modeling intercomparison: Photochemical box model simulation, Journal of Geophysical Research: Atmospheres, 108, n/a–n/a, https://doi.org/10.1029/2002JD002673, http://dx.doi.org/10.1029/2002JD002673, 4214, 2003.

Borbon, A., Ruiz, M., Bechara, J., Aumont, B., Chong, M., Huntrieser, H., Mari, C., Reeves, C. E., Scialom, G., Hamburger, T., Stark, H., Afif, C., Jambert, C., Mills, G., Schlager, H., and Perros, P. E.: Transport and chemistry of formaldehyde by mesoscale convective systems in West Africa during AMMA 2006: FORMALDEHYDE IN WEST AFRICA, Journal of Geophysical Research: Atmospheres, 117, n/a–n/a, https://doi.org/10.1029/2011JD017121, http://doi.wiley.com/10.1029/2011JD017121, 2012.

Butler, T. M., Taraborrelli, D., Brühl, C., Fischer, H., Harder, H., Martinez, M., Williams, J., Lawrence, M. G., and Lelieveld, J.: Improved simulation of isoprene oxidation chemistry with the ECHAM5/MESSy chemistry-climate model: lessons from the GABRIEL airborne field campaign, Atmospheric Chemistry and Physics, 8, 4529–4546, http://www.atmos-chem-phys.net/8/4529/2008/acp-8-4529-2008.html, 2008.

Chen, G., Xue, H., Feingold, G., and Zhou, X.: Vertical transport of pollutants by shallow cumuli from large eddy simulations, Atmospheric Chemistry and Physics, 12, 11 319–11 327, https://doi.org/10.5194/acp-12-11319-2012, http://www.atmos-chem-phys.net/12/11319/2012/, 2012.

Commane, R., Floquet, C. F. A., Ingham, T., Stone, D., Evans, M. J., and Heard, D. E.: Observations of OH and HO₂ radicals over West Africa, Atmospheric Chemistry and Physics, 10, 8783–8801, https://doi.org/10.5194/acp-10-8783-2010, http://www.atmos-chem-phys.net/10/8783/2010/, 2010.

Couvreux, F., Hourdin, F., and Rio, C.: Resolved Versus Parametrized Boundary-Layer Plumes. Part I: A Parametrization-Oriented Conditional Sampling in Large-Eddy Simulations, Boundary-Layer Meteorology, 134, 441–458, https://doi.org/10.1007/s10546-009-9456-5, http://link.springer.com/10.1007/s10546-009-9456-5, 2010.

Couvreux, F., Guichard, F., Gounou, A., Bouniol, D., Peyrillé, P., and Köhler, M.: Modelling of the Thermodynamical Diurnal Cycle in the Lower Atmosphere: A Joint Evaluation of Four Contrasted Regimes in the Tropics Over Land, Boundary-Layer Meteorology, 150, 185–214, https://doi.org/10.1007/s10546-013-9862-6, http://link.springer.com/10.1007/s10546-013-9862-6, 2014.

Cuxart, J., Bougeault, P., and Redelsperger, J.-L.: A turbulence scheme allowing for mesoscale and large-eddy simulations, Quarterly Journal of the Royal Meteorological Society, 126, 1–30, https://doi.org/10.1002/qj.49712656202, http://doi.wiley.com/10.1002/qj.49712656202, 2000.

Delon, C., Galy-Lacaux, C., Boone, A., Liousse, C., Serça, D., Adon, M., Diop, B., Akpo, A., Lavenu, F., Mougin, E., and others: Atmospheric nitrogen budget in Sahelian dry savannas, Atmospheric Chemistry and Physics, 10, 2691–2708, http://www.atmos-chem-phys.net/10/2691/2010/acp-10-2691-2010.html, 2010.

Di Carlo, P.: Missing OH Reactivity in a Forest: Evidence for Unknown Reactive Biogenic VOCs, Science, 304, 722–725, https://doi.org/10.1126/science.1094392, http://www.sciencemag.org/cgi/doi/10.1126/science.1094392, 2004.

Dlugi, R., Berger, M., Zelger, M., Hofzumahaus, A., Siese, M., Holland, F., Wisthaler, A., Grabmer, W., Hansel, A., Koppmann, R., Kramm, G., Möllmann-Coers, M., and Knaps, A.: Turbulent exchange and segregation of HO_x radicals and volatile organic compounds above a deciduous forest, Atmospheric Chemistry and Physics, 10, 6215–6235, https://doi.org/10.5194/acp-10-6215-2010, http://www.atmos-chem-phys.net/10/6215/2010/, 2010.

Ehhalt, D. H.: Photooxidation of trace gases in the troposphere Plenary Lecture, Physical Chemistry Chemical Physics, 1, 5401–5408, https://doi.org/10.1039/a905097c, http://xlink.rsc.org/?DOI=a905097c, 1999.

Ferreira, J., Reeves, C. E., Murphy, J. G., Garcia-Carreras, L., Parker, D. J., and Oram, D. E.: Isoprene emissions modelling for West Africa: MEGAN model evaluation and sensitivity analysis, Atmospheric Chemistry and Physics, 10, 8453–8467, https://doi.org/10.5194/acp-10-8453-2010, http://www.atmos-chem-phys.net/10/8453/2010/, 2010.

Gounou, A., Guichard, F., and Couvreux, F.: Observations of Diurnal Cycles Over a West African Meridional Transect: Pre-Monsoon and Full-Monsoon Seasons, Boundary-Layer Meteorology, 144, 329–357, https://doi.org/10.1007/s10546-012-9723-8, http://link.springer.com/10.1007/s10546-012-9723-8, 2012.

Griffin, R. J.: Secondary organic aerosol 1. Atmospheric chemical mechanism for production of molecular constituents, Journal of Geophysical Research, 107, https://doi.org/10.1029/2001JD000541, http://doi.wiley.com/10.1029/2001JD000541, 2002.

Groß, C. B. M., Dillon, T. J., Schuster, G., Lelieveld, J., and Crowley, J. N.: Direct Kinetic Study of OH and O $_3$ Formation in the Reaction of CH $_3$ C(O)O $_2$ with HO $_2$, The Journal of Physical Chemistry A, 118, 974–985, https://doi.org/10.1021/jp412380z, http://pubs.acs.org/doi/abs/10.1021/jp412380z, 2014.

Guenther, A., Karl, T., Harley, P., Wiedinmyer, C., Palmer, P. I., and Geron, C.: Estimates of global terrestrial isoprene emissions using MEGAN (Model of Emissions of Gases and Aerosols from Nature), Atmospheric Chemistry and Physics, 6, 3181–3210, https://doi.org/10.5194/acp-6-3181-2006, http://www.atmos-chem-phys.net/6/3181/2006/, 2006.

Guenther, A. B., Monson, R. K., and Fall, R.: Isoprene and monoterpene emission rate variability: observations with eucalyptus and emission rate algorithm development, Journal of Geophysical Research: Atmospheres, 96, 10 799–10 808, http://onlinelibrary.wiley.com/doi/10.1029/91JD00960/full, 1991.

Hannak, L., Knippertz, P., Fink, A. H., Kniffka, A., and Pante, G.: Why Do Global Climate Models Struggle to Represent Low-Level Clouds in the West African Summer Monsoon?, Journal of Climate, 30, 1665–1687, https://doi.org/10.1175/JCLI-D-16-0451.1, http://journals.ametsoc.org/doi/10.1175/JCLI-D-16-0451.1, 2017.

Hansen, R. F., Blocquet, M., Schoemaecker, C., Léonardis, T., Locoge, N., Fittschen, C., Hanoune, B., Stevens, P. S., Sinha, V., and Dusanter, S.: Intercomparison of the comparative reactivity method (CRM) and pump–probe technique for measuring total OH reactivity in an urban environment, Atmospheric Measurement Techniques, 8, 4243–4264, https://doi.org/10.5194/amt-8-4243-2015, http://www.atmos-meas-tech.net/8/4243/2015/, 2015a.

Hansen, R. F., Blocquet, M., Schoemaecker, C., Léonardis, T., Locoge, N., Fittschen, C., Hanoune, B., Stevens, P. S., Sinha, V., and Dusanter, S.: Intercomparison of the comparative reactivity method (CRM) and pump–probe technique for measuring total OH reac-

tivity in an urban environment, Atmospheric Measurement Techniques, 8, 4243–4264, https://doi.org/10.5194/amt-8-4243-2015, http://www.atmos-meas-tech.net/8/4243/2015/, 2015b.

Hasson, A. S., Tyndall, G. S., and Orlando, J. J.: A Product Yield Study of the Reaction of HO_2 Radicals with Ethyl Peroxy ($C_2H_5O_2$), Acetyl Peroxy ($CH_3C(O)O_2$), and Acetonyl Peroxy ($CH_3C(O)CH_2O_2$) Radicals, The Journal of Physical Chemistry A, 108, 5979–5989, https://doi.org/10.1021/jp048873t, http://pubs.acs.org/doi/abs/10.1021/jp048873t, 2004.

Jenkin, M. E., Hurley, M. D., and Wallington, T. J.: Investigation of the radical product channel of the CH3C(O)O2 + HO2 reaction in the gas phase, Physical Chemistry Chemical Physics, 9, 3149, https://doi.org/10.1039/b702757e, http://xlink.rsc.org/?DOI=b702757e, 2007.

Junker, C. and Liousse, C.: A global emission inventory of carbonaceous aerosol from historic records of fossil fuel and biofuel consumption for the period 1860–1997, Atmospheric Chemistry and Physics, 8, 1195–1207, https://doi.org/10.5194/acp-8-1195-2008, https://www.atmos-chem-phys.net/8/1195/2008/, 2008.

Kim, S.-W., Barth, M. C., and Trainer, M.: Influence of fair-weather cumulus clouds on isoprene chemistry: IMPACT OF SHALLOW CONVECTION ON ISOPRENE, Journal of Geophysical Research: Atmospheres, 117, n/a–n/a, https://doi.org/10.1029/2011JD017099, http://doi.wiley.com/10.1029/2011JD017099, 2012.

Kim, S.-W., Barth, M. C., and Trainer, M.: Impact of turbulent mixing on isoprene chemistry: IMPACT OF TURBULENCE ON ISOPRENE CHEMISTRY, Geophysical Research Letters, 43, 7701–7708, https://doi.org/10.1002/2016GL069752, http://doi.wiley.com/10.1002/2016GL069752, 2016.

Knippertz, P., Fink, A. H., Schuster, R., Trentmann, J., Schrage, J. M., and Yorke, C.: Ultra-low clouds over the southern West African monsoon region: ULTRA-LOW CLOUDS OVER WEST AFRICA, Geophysical Research Letters, 38, n/a–n/a, https://doi.org/10.1029/2011GL049278, http://doi.wiley.com/10.1029/2011GL049278, 2011.

Kovacs, T. A., Brune, W. H., Harder, H., Martinez, M., Simpas, J. B., Frost, G. J., Williams, E., Jobson, T., Stroud, C., Young, V., Fried, A., and Wert, B.: Direct measurements of urban OH reactivity during Nashville SOS in summer 1999, Journal of environmental monitoring: JEM, 5, 68–74, 2003.

Kubistin, D., Harder, H., Martinez, M., Rudolf, M., Sander, R., Bozem, H., Eerdekens, G., Fischer, H., Gurk, C., Klüpfel, T., Königstedt, R., Parchatka, U., Schiller, C. L., Stickler, A., Taraborrelli, D., Williams, J., and Lelieveld, J.: Hydroxyl radicals in the tropical troposphere over the Suriname rainforest: comparison of measurements with the box model MECCA, Atmospheric Chemistry and Physics, 10, 9705–9728, https://doi.org/10.5194/acp-10-9705-2010, http://www.atmos-chem-phys.net/10/9705/2010/, 2010.

Lafore, J. P., Stein, J., Asencio, N., Bougeault, P., Ducrocq, V., Duron, J., Fischer, C., Héreil, P., Mascart, P., Masson, V., Pinty, J. P., Redelsperger, J. L., Richard, E., and Vilà-Guerau de Arellano, J.: The Meso-NH Atmospheric Simulation System. Part I: adiabatic formulation and control simulations, Annales Geophysicae, 16, 90–109, https://doi.org/10.1007/s00585-997-0090-6, http://www.ann-geophys.net/16/90/1998/, 1998.

Lelieveld, J. and Crutzen, P.: Influences of cloud photochemical processes on tropospheric ozone, Nature, 343, 227–233, https://doi.org/10.1038/343227a0, http://www.nature.com/doifinder/10.1038/343227a0, 1990.

Lelieveld, J., Butler, T. M., Crowley, J. N., Dillon, T. J., Fischer, H., Ganzeveld, L., Harder, H., Lawrence, M. G., Martinez, M., Taraborrelli, D., and Williams, J.: Atmospheric oxidation capacity sustained by a tropical forest, Nature, 452, 737–740, https://doi.org/10.1038/nature06870, http://www.nature.com/doifinder/10.1038/nature06870, 2008.

Lelieveld, J., Gromov, S., Pozzer, A., and Taraborrelli, D.: Global tropospheric hydroxyl distribution, budget and reactivity, Atmospheric Chemistry and Physics, 16, 12 477–12 493, https://doi.org/10.5194/acp-16-12477-2016, http://www.atmos-chem-phys.net/16/12477/2016/, 2016.

Li, Y., Barth, M. C., Chen, G., Patton, E. G., Kim, S.-W., Wisthaler, A., Mikoviny, T., Fried, A., Clark, R., and Steiner, A. L.: Large-eddy simulation of biogenic VOC chemistry during the DISCOVER-AQ 2011 campaign: LARGE-EDDY SIMULATION OF BVOC CHEMISTRY, Journal of Geophysical Research: Atmospheres, 121, 8083–8105, https://doi.org/10.1002/2016JD024942, http://doi.wiley.com/10.1002/2016JD024942, 2016.

Mamtimin, B., Meixner, F. X., Behrendt, T., Badawy, M., and Wagner, T.: The contribution of soil biogenic NO and HONO emissions from a managed hyperarid ecosystem to the regional NO_{<i>x</i>} emissions during growing season, Atmospheric Chemistry and Physics, 16, 10 175–10 194, https://doi.org/10.5194/acp-16-10175-2016, http://www.atmos-chem-phys.net/16/10175/2016/, 2016.

Mao, J., Ren, X., Chen, S., Brune, W. H., Chen, Z., Martinez, M., Harder, H., Lefer, B., Rappenglück, B., Flynn, J., and Leuchner, M.: Atmospheric oxidation capacity in the summer of Houston 2006: Comparison with summer measurements in other metropolitan studies, Atmospheric Environment, 44, 4107–4115, https://doi.org/10.1016/j.atmosenv.2009.01.013, http://linkinghub.elsevier.com/retrieve/pii/S1352231009000351, 2010.

Masson, V., Le Moigne, P., Martin, E., Faroux, S., Alias, A., Alkama, R., Belamari, S., Barbu, A., Boone, A., Bouyssel, F., Brousseau, P., Brun, E., Calvet, J.-C., Carrer, D., Decharme, B., Delire, C., Donier, S., Essaouini, K., Gibelin, A.-L., Giordani, H., Habets, F., Jidane, M., Kerdraon, G., Kourzeneva, E., Lafaysse, M., Lafont, S., Lebeaupin Brossier, C., Lemonsu, A., Mahfouf, J.-F., Marguinaud, P., Mokhtari, M., Morin, S., Pigeon, G., Salgado, R., Seity, Y., Taillefer, F., Tanguy, G., Tulet, P., Vincendon, B., Vionnet, V., and Voldoire, A.: The SURFEXv7.2 land and ocean surface platform for coupled or offline simulation of earth surface variables and fluxes, Geoscientific Model Development, 6, 929–960, https://doi.org/10.5194/gmd-6-929-2013, http://www.geosci-model-dev.net/6/929/2013/, 2013.

Mauldin, R. L., Madronich, S., Flocke, S. J., Eisele, F. L., Frost, G. J., and Prevot, A. S. H.: New insights on OH: Measurements around and in clouds, Geophysical Research Letters, 24, 3033–3036, https://doi.org/10.1029/97GL02983, http://doi.wiley.com/10.1029/97GL02983, 1997.

Mogensen, D., Smolander, S., Sogachev, A., Zhou, L., Sinha, V., Guenther, A., Williams, J., Nieminen, T., Kajos, M. K., Rinne, J., Kulmala, M., and Boy, M.: Modelling atmospheric OH-reactivity in a boreal forest ecosystem, Atmospheric Chemistry and Physics, 11, 9709–9719, https://doi.org/10.5194/acp-11-9709-2011, http://www.atmos-chem-phys.net/11/9709/2011/, 2011.

Molemaker, M. J. and Vilà-Guerau de Arellano, J.: Control of Chemical Reactions by Convective Turbulence in the Boundary Layer, Journal of the Atmospheric Sciences, 55, 568–579, https://doi.org/10.1175/1520-0469(1998)055<0568:COCRBC>2.0.CO;2, http://journals.ametsoc.org/doi/abs/10.1175/1520-0469%281998%29055%3C0568%3ACOCRBC%3E2.0.CO%3B2, 1998.

Murphy, J. G., Oram, D. E., and Reeves, C. E.: Measurements of volatile organic compounds over West Africa, Atmospheric Chemistry and Physics, 10, 5281–5294, https://doi.org/10.5194/acp-10-5281-2010, http://www.atmos-chem-phys.net/10/5281/2010/, 2010.

Nölscher, A. C., Williams, J., Sinha, V., Custer, T., Song, W., Johnson, A. M., Axinte, R., Bozem, H., Fischer, H., Pouvesle, N., Phillips, G., Crowley, J. N., Rantala, P., Rinne, J., Kulmala, M., Gonzales, D., Valverde-Canossa, J., Vogel, A., Hoffmann, T., Ouwersloot, H. G., Vilà-Guerau de Arellano, J., and Lelieveld, J.: Summertime total OH reactivity measurements from boreal forest during HUMPPA-COPEC 2010, Atmospheric Chemistry and Physics, 12, 8257–8270, https://doi.org/10.5194/acp-12-8257-2012, http://www.atmos-chem-phys.net/12/8257/2012/, 2012.

Nölscher, A. C., Yañez-Serrano, A. M., Wolff, S., de Araujo, A. C., Lavrič, J. V., Kesselmeier, J., and Williams, J.: Unexpected seasonality in quantity and composition of Amazon rainforest air reactivity, Nature Communications, 7, 10 383, https://doi.org/10.1038/ncomms10383, http://www.nature.com/doifinder/10.1038/ncomms10383, 2016.

Ouwersloot, H. G., Vilà-Guerau de Arellano, J., van Heerwaarden, C. C., Ganzeveld, L. N., Krol, M. C., and Lelieveld, J.: On the segregation of chemical species in a clear boundary layer over heterogeneous land surfaces, Atmos. Chem. Phys., 11, 10 681–10 704, https://doi.org/10.5194/acp-11-10681-2011, http://www.atmos-chem-phys.net/11/10681/2011/, 2011.

Peeters, J., Nguyen, T. L., and Vereecken, L.: HOx radical regeneration in the oxidation of isoprene, Physical Chemistry Chemical Physics, 11, 5935, https://doi.org/10.1039/b908511d, http://xlink.rsc.org/?DOI=b908511d, 2009.

Pinty, J.-P. and Jabouille, P.: 6B. 4 A MIXED-PHASE CLOUD PARAMETERIZATION FOR USE IN A MESOSCALE NON-HYDROSTATIC MODEL: SIMULATIONS OF A SQUALL LINE AND OF OROGRAPHIC PRECIPITATION, pp. 217–220, http://195.83.22.22/mesonh/dir_publication/pinty_jabouille_ams_ccp1998.pdf, 1998.

Pugh, T. A. M., MacKenzie, A. R., Hewitt, C. N., Langford, B., Edwards, P. M., Furneaux, K. L., Heard, D. E., Hopkins, J. R., Jones, C. E., Karunaharan, A., Lee, J., Mills, G., Misztal, P., Moller, S., Monks, P. S., and Whalley, L. K.: Simulating atmospheric composition over a South-East Asian tropical rainforest: performance of a chemistry box model, Atmospheric Chemistry and Physics, 10, 279–298, https://doi.org/10.5194/acp-10-279-2010, http://www.atmos-chem-phys.net/10/279/2010/, 2010.

Ramasamy, S., Ida, A., Jones, C., Kato, S., Tsurumaru, H., Kishimoto, I., Kawasaki, S., Sadanaga, Y., Nakashima, Y., Nakayama, T., Matsumi, Y., Mochida, M., Kagami, S., Deng, Y., Ogawa, S., Kawana, K., and Kajii, Y.: Total OH reactivity measurement in a BVOC dominated temperate forest during a summer campaign, 2014, Atmospheric Environment, 131, 41–54, https://doi.org/10.1016/j.atmosenv.2016.01.039, http://linkinghub.elsevier.com/retrieve/pii/S135223101630053X, 2016.

Redelsperger, J.-L., Thorncroft, C. D., Diedhiou, A., Lebel, T., Parker, D. J., and Polcher, J.: African Monsoon Multidisciplinary Analysis: An International Research Project and Field Campaign, Bulletin of the American Meteorological Society, 87, 1739–1746, https://doi.org/10.1175/BAMS-87-12-1739, http://journals.ametsoc.org/doi/abs/10.1175/BAMS-87-12-1739, 2006.

Reeves, C. E., Formenti, P., Afif, C., Ancellet, G., Attié, J.-L., Bechara, J., Borbon, A., Cairo, F., Coe, H., Crumeyrolle, S., Fierli, F., Flamant, C., Gomes, L., Hamburger, T., Jambert, C., Law, K. S., Mari, C., Jones, R. L., Matsuki, A., Mead, M. I., Methven, J., Mills, G. P., Minikin, A., Murphy, J. G., Nielsen, J. K., Oram, D. E., Parker, D. J., Richter, A., Schlager, H., Schwarzenboeck, A., and Thouret, V.: Chemical and aerosol characterisation of the troposphere over West Africa during the monsoon period as part of AMMA, Atmospheric Chemistry and Physics, 10, 7575–7601, https://doi.org/10.5194/acp-10-7575-2010, http://www.atmos-chem-phys.net/10/7575/2010/, 2010.

Ren, X.: OH and HO2 Chemistry in the urban atmosphere of New York City, Atmospheric Environment, 37, 3639–3651, https://doi.org/10.1016/S1352-2310(03)00459-X, http://linkinghub.elsevier.com/retrieve/pii/S135223100300459X, 2003.

Sadanaga, Y.: The importance of NO_2 and volatile organic compounds in the urban air from the viewpoint of the OH reactivity, Geophysical Research Letters, 31, https://doi.org/10.1029/2004GL019661, http://doi.wiley.com/10.1029/2004GL019661, 2004.

Sadanaga, Y., Yoshino, A., Kato, S., Yoshioka, A., Watanabe, K., Miyakawa, Y., Hayashi, I., Ichikawa, M., Matsumoto, J., Nishiyama, A., Akiyama, N., Kanaya, Y., and Kajii, Y.: The importance of NO2 and volatile organic compounds in the urban air from the viewpoint of the OH reactivity, Geophysical Research Letters, 31, L08 102, https://doi.org/10.1029/2004GL019661, http://onlinelibrary.wiley.com/doi/10.1029/2004GL019661/abstract, 2004.

Saxton, J. E., Lewis, A. C., Kettlewell, J. H., Ozel, M. Z., Gogus, F., Boni, Y., Korogone, S. O. U., and Serça, D.: Isoprene and monoterpene measurements in a secondary forest in northern Benin, Atmospheric Chemistry and Physics, 7, 4095–4106, http://www.atmos-chem-phys.net/7/4095/2007/acp-7-4095-2007.pdf, 2007.

Schrage, J. M. and Fink, A. H.: Nocturnal Continental Low-Level Stratus over Tropical West Africa: Observations and Possible Mechanisms Controlling Its Onset, Monthly Weather Review, 140, 1794–1809, https://doi.org/10.1175/MWR-D-11-00172.1, http://journals.ametsoc.org/doi/abs/10.1175/MWR-D-11-00172.1, 2012.

Schrage, J. M., Augustyn, S., and Fink, A. H.: Nocturnal stratiform cloudiness during the West African monsoon, Meteorology and Atmospheric Physics, 95, 73–86, https://doi.org/10.1007/s00703-006-0194-7, http://link.springer.com/10.1007/s00703-006-0194-7, 2007.

Schumann, U.: Large-eddy simulation of turbulent diffusion with chemical reactions in the convective boundary layer, Atmospheric Environment (1967), 23, 1713–1727, https://doi.org/10.1016/0004-6981(89)90056-5, http://www.sciencedirect.com/science/article/pii/0004698189900565, 1989.

Shirley, T. R., Brune, W. H., Ren, X., Mao, J., Lesher, R., Cardenas, B., Volkamer, R., Molina, L. T., Molina, M. J., Lamb, B., Velasco, E., Jobson, T., and Alexander, M.: Atmospheric oxidation in the Mexico City Metropolitan Area (MCMA) during April 2003, Atmospheric Chemistry and Physics, 6, 2753–2765, https://doi.org/10.5194/acp-6-2753-2006, http://www.atmos-chem-phys.net/6/2753/2006/, 2006.

Sindelarova, K., Granier, C., Bouarar, I., Guenther, A., Tilmes, S., Stavrakou, T., Müller, J.-F., Kuhn, U., Stefani, P., and Knorr, W.: Global data set of biogenic VOC emissions calculated by the MEGAN model over the last 30 years, Atmospheric Chemistry and Physics, 14, 9317–9341, https://doi.org/10.5194/acp-14-9317-2014, http://www.atmos-chem-phys.net/14/9317/2014/, 2014.

Sinha, V., Williams, J., Crowley, J. N., and Lelieveld, J.: The Comparative Reactivity Method – a new tool to measure total OH Reactivity in ambient air, Atmospheric Chemistry and Physics, 8, 2213–2227, https://doi.org/10.5194/acp-8-2213-2008, http://www.atmos-chem-phys.net/8/2213/2008/, 2008.

Sinha, V., Williams, J., Lelieveld, J., Ruuskanen, T., Kajos, M., Patokoski, J., Hellen, H., Hakola, H., Mogensen, D., Boy, M., Rinne, J., and Kulmala, M.: OH Reactivity Measurements within a Boreal Forest: Evidence for Unknown Reactive Emissions, Environmental Science & Technology, 44, 6614–6620, https://doi.org/10.1021/es101780b, http://pubs.acs.org/doi/abs/10.1021/es101780b, 2010.

Stewart, D. J., Taylor, C. M., Reeves, C. E., and McQuaid, J. B.: Biogenic nitrogen oxide emissions from soils: impact on NO_x and ozone over west Africa during AMMA (African Monsoon Multidisciplinary Analysis): observational study, Atmospheric Chemistry and Physics, 8, 2285–2297, https://doi.org/10.5194/acp-8-2285-2008, http://www.atmos-chem-phys.net/8/2285/2008/, 2008.

Stone, D., Evans, M. J., Edwards, P. M., Commane, R., Ingham, T., Rickard, A. R., Brookes, D. M., Hopkins, J., Leigh, R. J., Lewis, A. C., Monks, P. S., Oram, D., Reeves, C. E., Stewart, D., and Heard, D. E.: Isoprene oxidation mechanisms: measurements and modelling of OH and HO₂ over a South-East Asian tropical rainforest during the OP3 field campaign, Atmospheric Chemistry and Physics, 11, 6749–6771, https://doi.org/10.5194/acp-11-6749-2011, http://www.atmos-chem-phys.net/11/6749/2011/, 2011.

Thouret, V., Saunois, M., Minga, A., Mariscal, A., Sauvage, B., Solete, A., Agbangla, D., Nédélec, P., Mari, C., Reeves, C. E., and Schlager, H.: An overview of two years of ozone radio soundings over Cotonou as part of AMMA, Atmospheric Chemistry and Physics, 9, 6157–6174, https://doi.org/10.5194/acp-9-6157-2009, http://www.atmos-chem-phys.net/9/6157/2009/, 2009.

Tulet, P., Grini, A., Griffin, R. J., and Petitcol, S.: ORILAM-SOA: A computationally efficient model for predicting secondary organic aerosols in three-dimensional atmospheric models, Journal of Geophysical Research, 111, https://doi.org/10.1029/2006JD007152, http://doi.wiley.com/10.1029/2006JD007152, 2006.

Vilà-Guerau de Arellano, J. and Cuijpers, J. W. M.: The Chemistry of a Dry Cloud: The Effects of Radiation and Turbulence, Journal of the Atmospheric Sciences, 57, 1573–1584, https://doi.org/10.1175/1520-0469(2000)057<1573:TCOADC>2.0.CO;2, http://journals.ametsoc.org/doi/abs/10.1175/1520-0469%282000%29057%3C1573%3ATCOADC%3E2.0.CO%3B2, 2000.

Vilà-Guerau de Arellano, J., Kim, S.-W., Barth, M. C., and Patton, E. G.: Transport and chemical transformations influenced by shallow cumulus over land, Atmospheric Chemistry and Physics, 5, 3219–3231, https://doi.org/10.5194/acp-5-3219-2005, http://www.atmos-chem-phys.net/5/3219/2005/, 2005.

Vinuesa, J.-F. and Vilà-Guerau de Arellano, J.: Introducing effective reaction rates to account for the inefficient mixing of the convective boundary layer, Atmospheric Environment, 39, 445–461, https://doi.org/10.1016/j.atmosenv.2004.10.003, http://linkinghub.elsevier.com/retrieve/pii/S1352231004009264, 2005.

Whalley, L. K., Edwards, P. M., Furneaux, K. L., Goddard, A., Ingham, T., Evans, M. J., Stone, D., Hopkins, J. R., Jones, C. E., Karunaharan, A., Lee, J. D., Lewis, A. C., Monks, P. S., Moller, S. J., and Heard, D. E.: Quantifying the magnitude of a missing hydroxyl radical source in a tropical rainforest, Atmospheric Chemistry and Physics, 11, 7223–7233, https://doi.org/10.5194/acp-11-7223-2011, http://www.atmos-chem-phys.net/11/7223/2011/, 2011.

Whalley, L. K., Stone, D., Bandy, B., Dunmore, R., Hamilton, J. F., Hopkins, J., Lee, J. D., Lewis, A. C., and Heard, D. E.: Atmospheric OH reactivity in central London: observations, model predictions and estimates of in situ ozone production, Atmospheric Chemistry and Physics, 16, 2109–2122, https://doi.org/10.5194/acp-16-2109-2016, http://www.atmos-chem-phys.net/16/2109/2016/, 2016.

Williams, I., Revitt, D., and Hamilton, R.: A comparison of carbonyl compound concentrations at urban roadside and indoor sites, Science of The Total Environment, 189-190, 475–483, https://doi.org/10.1016/0048-9697(96)05248-5, http://linkinghub.elsevier.com/retrieve/pii/0048969796052485, 1996.

Williams, J. and Brune, W.: A roadmap for OH reactivity research, Atmospheric Environment, 106, 371–372, https://doi.org/10.1016/j.atmosenv.2015.02.017, http://linkinghub.elsevier.com/retrieve/pii/S1352231015001363, 2015.

Williams, J., Keßel, S. U., Nölscher, A. C., Yang, Y., Lee, Y., Yáñez-Serrano, A. M., Wolff, S., Kesselmeier, J., Klüpfel, T., Lelieveld, J., and Shao, M.: Opposite OH reactivity and ozone cycles in the Amazon rainforest and megacity Beijing: Subversion of biospheric oxidant control by anthropogenic emissions, Atmospheric Environment, 125, 112–118, https://doi.org/10.1016/j.atmosenv.2015.11.007, http://linkinghub.elsevier.com/retrieve/pii/S1352231015305161, 2016.

Winiberg, F. A. F., Dillon, T. J., Orr, S. C., Groß, C. B. M., Bejan, I., Brumby, C. A., Evans, M. J., Smith, S. C., Heard, D. E., and Seakins, P. W.: Direct measurements of OH and other product yields from the HO_2 + $CH_3C(O)O_2$ reaction, Atmospheric Chemistry and Physics, 16, 4023–4042, https://doi.org/10.5194/acp-16-4023-2016, http://www.atmos-chem-phys.net/16/4023/2016/, 2016.

Wyngaard, J. C. and Brost, R. A.: Top-Down and Bottom-Up Diffusion of a Scalar in the Convective Boundary Layer, Journal of the Atmospheric Sciences, 41, 102–112, https://doi.org/10.1175/1520-0469(1984)041<0102:TDABUD>2.0.CO;2, https://doi.org/10.1175/1520-0469(1984)041<0102:TDABUD>2.0.CO;2, 1984.

Yang, Y., Shao, M., Wang, X., Nölscher, A. C., Kessel, S., Guenther, A., and Williams, J.: Towards a quantitative understanding of total OH reactivity: A review, Atmospheric Environment, 134, 147–161, https://doi.org/10.1016/j.atmosenv.2016.03.010, http://linkinghub.elsevier.com/retrieve/pii/S1352231016301819, 2016.

Yienger, J. J. and Levy, H.: Empirical model of global soil-biogenic NO $_x$ emissions, Journal of Geophysical Research, 100, 11 447, https://doi.org/10.1029/95JD00370, http://doi.wiley.com/10.1029/95JD00370, 1995.

Zannoni, N., Gros, V., Lanza, M., Sarda, R., Bonsang, B., Kalogridis, C., Preunkert, S., Legrand, M., Jambert, C., Boissard, C., and Lathiere, J.: OH reactivity and concentrations of biogenic volatile organic compounds in a Mediterranean forest of downy oak trees, Atmospheric Chemistry and Physics, 16, 1619–1636, https://doi.org/10.5194/acp-16-1619-2016, http://www.atmos-chem-phys.net/16/1619/2016/, 2016.

Zhang, Y., Gao, Z., Li, D., Li, Y., Zhang, N., Zhao, X., and Chen, J.: On the computation of planetary boundary-layer height using the bulk Richardson number method, Geoscientific Model Development, 7, 2599–2611, https://doi.org/10.5194/gmd-7-2599-2014, http://www.geosci-model-dev.net/7/2599/2014/, 2014.

Atmos. Chem. Phys. Discuss., https://doi.org/10.5194/acp-2017-969
Manuscript under review for journal Atmos. Chem. Phys.
Discussion started: 20 November 2017

Atmospheric Chemistry and Physics Discussions

Table 1. Initial vertical profiles of mixing ratios and associated profiles. Number in brackets refers to (1) uniform profile, (2) stratospheric profile (initial profile multiplied by 1 from 0 to 2000m, then by 0.5 from 3000m to 13000m, by 0.75 at 14000m and 1 above), (3) boundary-layer profile (multiplied by 1 from 0 to 1000m, by 0.10 from 2000 to 13000m and 0.05 above). Chemical names are those used in the ReLACS3 chemical mechanism

Species	Initial mixing ratio	Species	Initial mixing ratio
O_3	21.19 ppb (2)	HO_2	2.48 ppt (1)
OH	0.07 ppt (1)	NO	55.25 ppt (2)
CO	149.23 ppb (3)	HCHO	747.47 ppt (3)
ALD2	896.82 ppt (3)	PAN2	35.70 ppt (3)
ALKL	282.90 ppt (3)	ALKM	3.67 ppt (3)
ALKH	0.60 ppt (3)	ETHE	277.12 ppt (3)
OLEL	104.71 ppt (3)	OLEH	0.94 ppt (3)
ISOP	1.23 ppb (3)	AROH	53.29 ppt (3)
AROL	14.11 ppt (3)	AROO	4.66 ppt (3)
ARAC+	0.69 ppt (3)	ARAL	1.98 ppt (3)
MEOH	564.54 ppt (3)	KETL	72.69 ppt (3)
MVK	537.74 ppt (3)	MCR	268.87 ppt (3)

Atmos. Chem. Phys. Discuss., https://doi.org/10.5194/acp-2017-969
Manuscript under review for journal Atmos. Chem. Phys.
Discussion started: 20 November 2017

Atmospheric Chemistry and Physics Discussions

Table 2. Emissions values for the biogenic and the anthropogenic cases, in kg.m^2.s^{-1}. For compounds in bold character, Gaussian shape emissions have been prescribed and only the maximum value is indicated here. Please see text for details.

Chemical species	Molar mass ($g.mol^{-1}$)	Biogenic patch emissions ($kg.m^{-2}.s^{-1}$)	Anthropogenic patch emissions ($kg.m^{-2}.s^{-1}$)
NO	30	$2.23 * 10^{-11}$	$5.68 * 10^{-10}$
NO_2	46	-	$2.44 * 10^{-10}$
CO	28	$2.13 * 10^{-11}$	$2.43 * 10^{-08}$
ETHE	28	$7.72 * 10^{-12}$	$8.06 * 10^{-10}$
OLEL	70	$3.26 * 10^{-12}$	$8.68 * 10^{-10}$
OLEH	126	$4.20 * 10^{-14}$	$1.91 * 10^{-11}$
ALKL	72	$2.72 * 10^{-14}$	$3.92 * 10^{-10}$
ALKM	128	$6.13 * 10^{-15}$	$1.31 * 10^{-10}$
ALKH	226	$8.76 * 10^{-16}$	$2.16 * 10^{-11}$
AROH	134	$2.75 * 10^{-13}$	$2.95 * 10^{-10}$
AROL	120	-	$1.98 * 10^{-10}$
AROO	122	-	$8.94 * 10^{-11}$
ARAC+	136	-	$1.32 * 10^{-11}$
ARAL	120	-	$3.81 * 10^{-11}$
ALD2	86	$2.99 * 10^{-12}$	$2.41 * 10^{-10}$
HCHO	30	$8.32 * 10^{-13}$	$8.39 * 10^{-11}$
ACID	74	-	$1.12 * 10^{-10}$
ORA1	46	$6.24 * 10^{-13}$	$5.75 * 10^{-10}$
ORA2	60	$6.24 * 10^{-13}$	$6.01 * 10^{-10}$
KETL	86	$6.80 * 10^{-13}$	$8.04 * 10^{-12}$
KETH	114	$2.51 * 10^{-14}$	$4.14 * 10^{-13}$
MEOH	32	$3.61 * 10^{-11}$	$2.64 * 10^{-11}$
ETOH	46	$2.15 * 10^{-12}$	$2.95 * 10^{-10}$
ALCH	102	-	$1.45 * 10^{-10}$
ISOP	68	$2.76 * 10^{-10}$	-
BIOL	154	$3.29 * 10^{-11}$	-
BIOH	88	$4.94 * 10^{-11}$	-
SO_2	64	-	$1.60 * 10^{-10}$
NH_3	17	-	$6.02 * 10^{-11}$
MTBE	88	-	$2.30 * 10^{-10}$

Atmos. Chem. Phys. Discuss., https://doi.org/10.5194/acp-2017-969
Manuscript under review for journal Atmos. Chem. Phys.
Discussion started: 20 November 2017

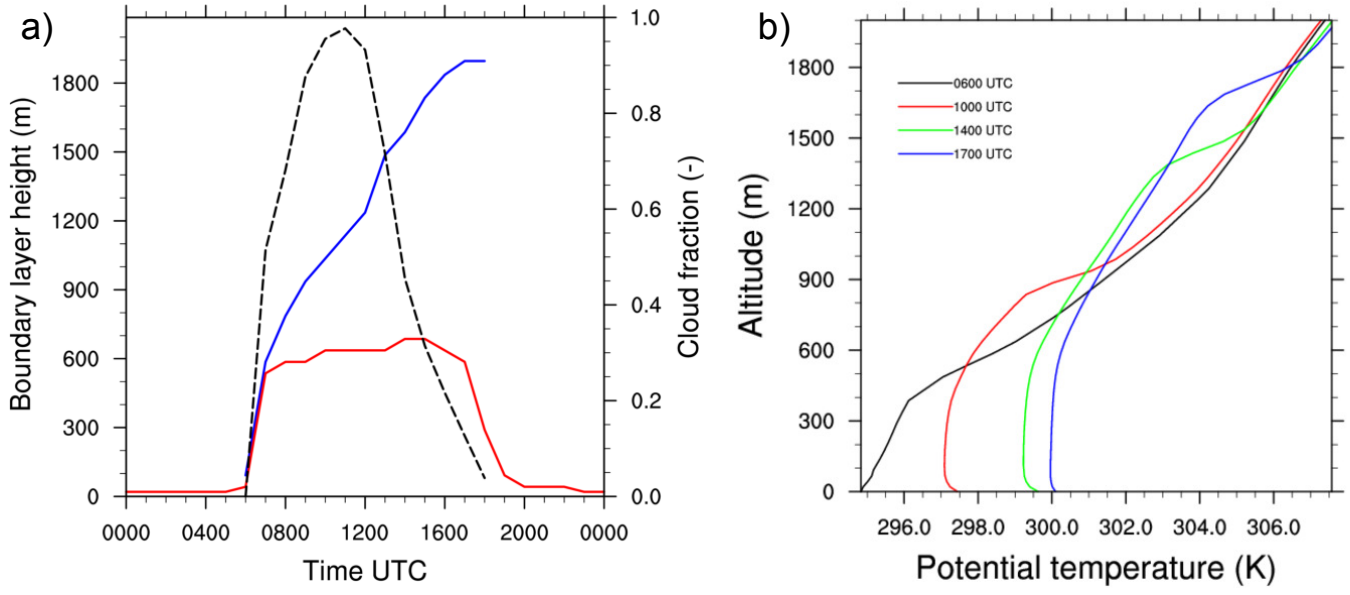

Figure 1. (a) Cloud fraction (dotted black) and boundary layer height diurnal evolution computed from the bulk-Richardson method (red) and tracer method (blue), (b) potential temperature vertical profiles at 0600 (black), 1000 (red), 1400 (green) and 1700 UTC (blue)

Atmos. Chem. Phys. Discuss., https://doi.org/10.5194/acp-2017-969
Manuscript under review for journal Atmos. Chem. Phys.
Discussion started: 20 November 2017

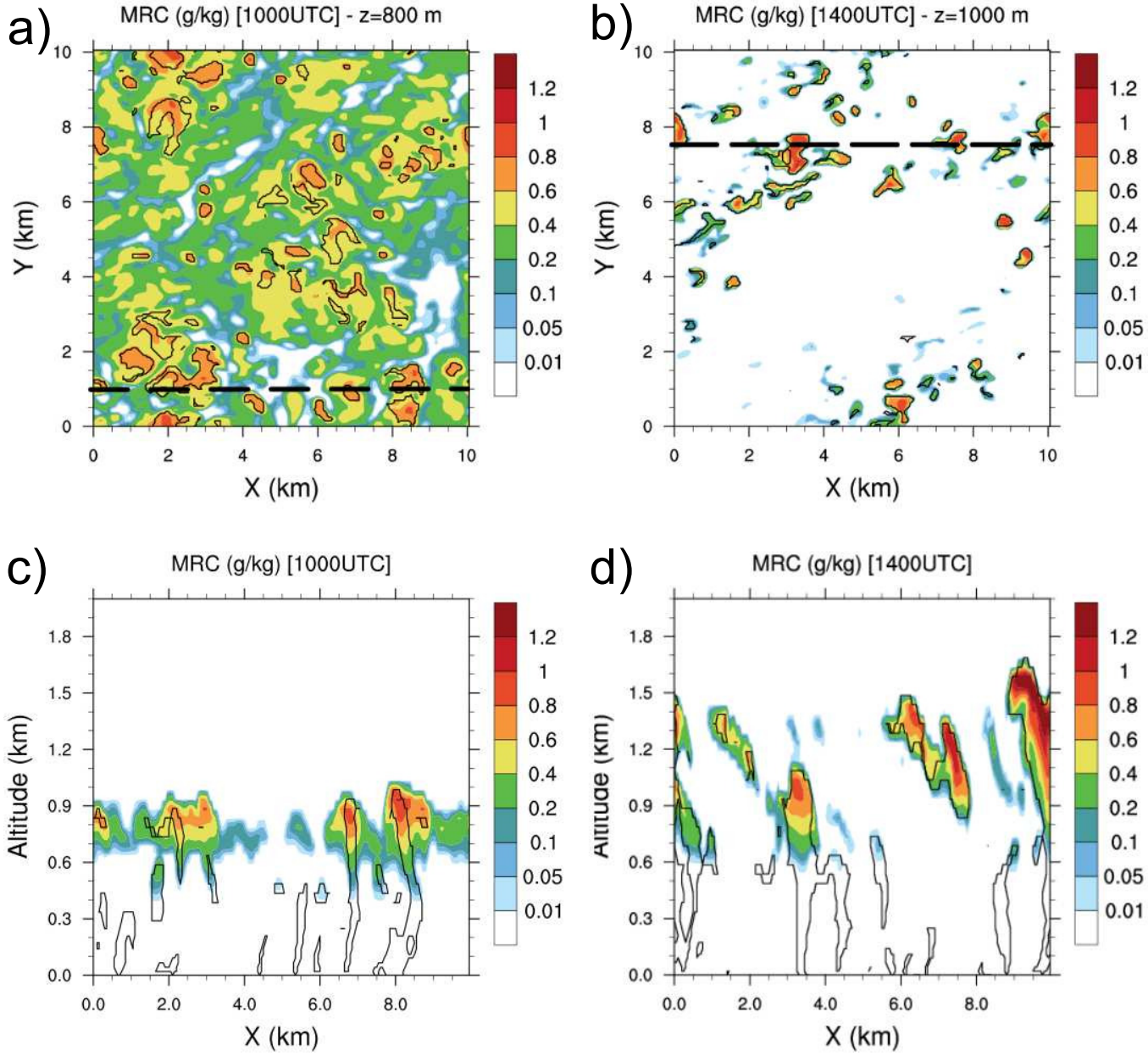

Figure 2. (a) Cloud water mixing ratio horizontal cross-sections at 1000 UTC and 800m height and (b) at 1400 UTC and 1000m height . Black dashed lines represent the vertical cross-sections at (c) 1000 UTC and y=1km and at (d) 1400 UTC and y=7.5km. Black isolines denote thermals identified by the conditional sampling method.

Atmos. Chem. Phys. Discuss., https://doi.org/10.5194/acp-2017-969
Manuscript under review for journal Atmos. Chem. Phys.
Discussion started: 20 November 2017

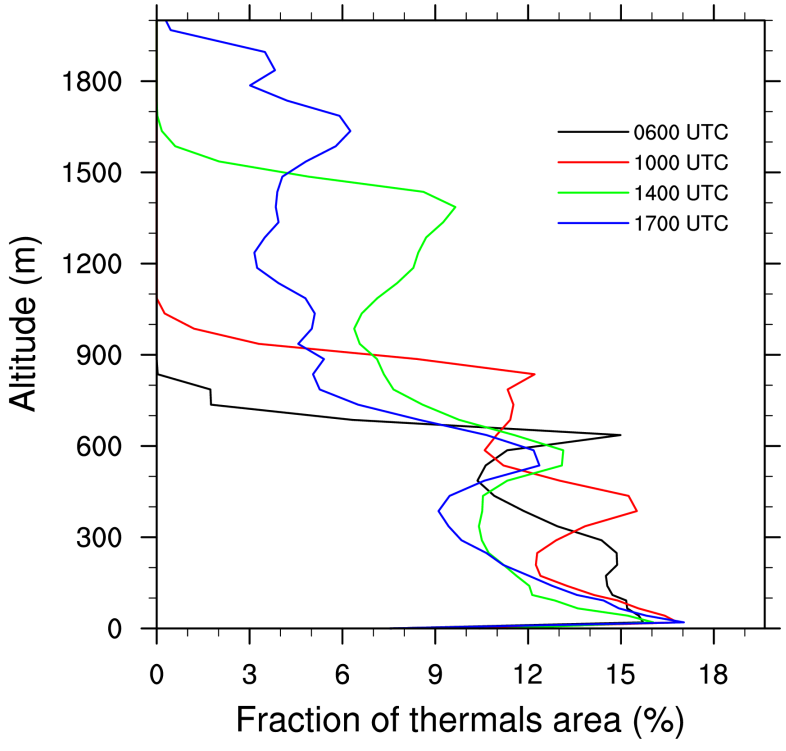

Figure 3. Vertical profiles of the fraction occupied by thermals at 0600 (black), 1000 (red), 1400 (green) and 1700 UTC (blue).

Atmos. Chem. Phys. Discuss., https://doi.org/10.5194/acp-2017-969
Manuscript under review for journal Atmos. Chem. Phys.
Discussion started: 20 November 2017

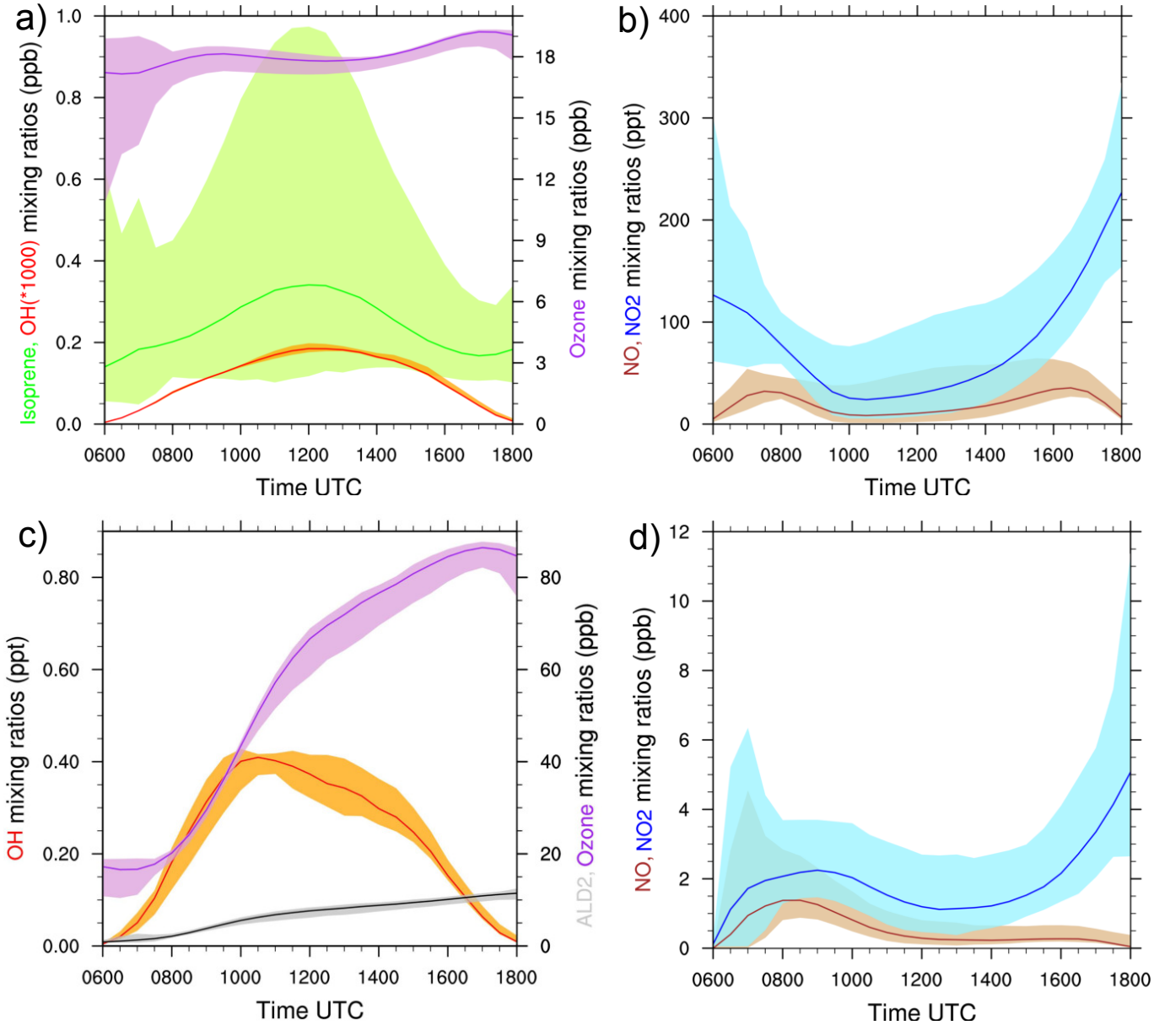

Figure 4. (a)-(b) LES simulated diurnal cycles for isoprene (green), OH (red), ozone (purple), (c)-(d) ALD2 (grey), NO (brown) and NO_2 (blue). (a)-(b) corresponds to the biogenic environment, (c)-(d) to the anthropogenic environment. The shaded areas denotes the minimum and the maximum of mean vertical profiles between the surface and 600m height, and the colored lines correspond to the average of these profiles

Atmos. Chem. Phys. Discuss., https://doi.org/10.5194/acp-2017-969
Manuscript under review for journal Atmos. Chem. Phys.
Discussion started: 20 November 2017

Atmospheric Chemistry and Physics Discussions

Table 3. Measurements collected during the AMMA campaign over forested area (upper part) and over cities (lower part). The last column corresponds to the concerned period.

Species	Mixing ratio	Altitude	Location	References	Comments
O3	24 ppbv	500 m	10°N	Commane et al. (2010)	1340 UTC - 17/08
	25 ppbv	<900 hPa	10°N	Reeves et al. (2010)	Median value (20/07 - 21/08)
	25-30 ppbv	300 - 1700 m	12-13°N	Borbon et al. (2012)	0800 -1800 UTC
	22 ppbv	<700 m	7.2-13.1°N	Murphy et al. (2010)	Mean value (17/07 - 17/08)
Isoprene	1.2 ppbv	<700 m	10°N	Ferreira et al. (2010)	1345 UTC - 17/08
	0.604 ppbv	<700 m	7.2-13.1°N	Murphy et al. (2010)	Mean value (17/07 - 17/08)
	1 - 1.5 ppbv	400 -1450 m	10°N		1200 UTC - 17/08
	0.2-1.5 ppbv	Surface	9.42°N;1,44°E	Saxton et al. (2007)	Composite diurnal cycle (07/06 - 13/06)
OH	0.05 - 0.15 pptv	500 m	10°N	Commane et al. (2010)	1345 UTC - 17/08
NO_x	0.2 ppbv	<900 hPa	10°N	Reeves et al. (2010)	Median value (20/07 - 21/08)
	0.1 ppbv	<700 m	9°N	Delon et al. (2010)	Mean value (05/08 - 17/08)
O3	40 ppbv	<2km	Cotonou	Ancellet et al. (2009)	08/19 p.m. flight
	24-30 ppbv	0-2 km	Cotonou	Thouret et al. (2009)	Mean value (August 2006)
	26 ppbv	<700m	Lagos	Murphy et al. (2010)	B229 flight - Mean value (17/07 - 17/08)
	31 ppbv		Niamey		
NOx	1 ppbv	<2km	Cotonou	Ancellet et al. (2009)	08/19 p.m. flight
OH	0-0.5 pptv	500m	Lagos	Commane et al. (2010)	B229 flight

Atmos. Chem. Phys. Discuss., https://doi.org/10.5194/acp-2017-969
Manuscript under review for journal Atmos. Chem. Phys.
Discussion started: 20 November 2017

Atmospheric Chemistry and Physics Discussions

Table 4. Simulated Damkhöler number of chemical species averaged from the surface to 0.6 km at 1200 UTC for the two cases calculated with $\tau_{turb} \approx 20$ mn.

	Damkhöler number (unitless)	
	Biogenic case	Anthropogenic case
OH	4402.7	12002.5
HO_2	50.4	137.5
ISOP	0.54	1.08
O_3	0.66	0.79
NO	80.2	81.0
NO_2	24.3	17.9
ALD2	0.086	0.17

Atmos. Chem. Phys. Discuss., https://doi.org/10.5194/acp-2017-969
Manuscript under review for journal Atmos. Chem. Phys.
Discussion started: 20 November 2017

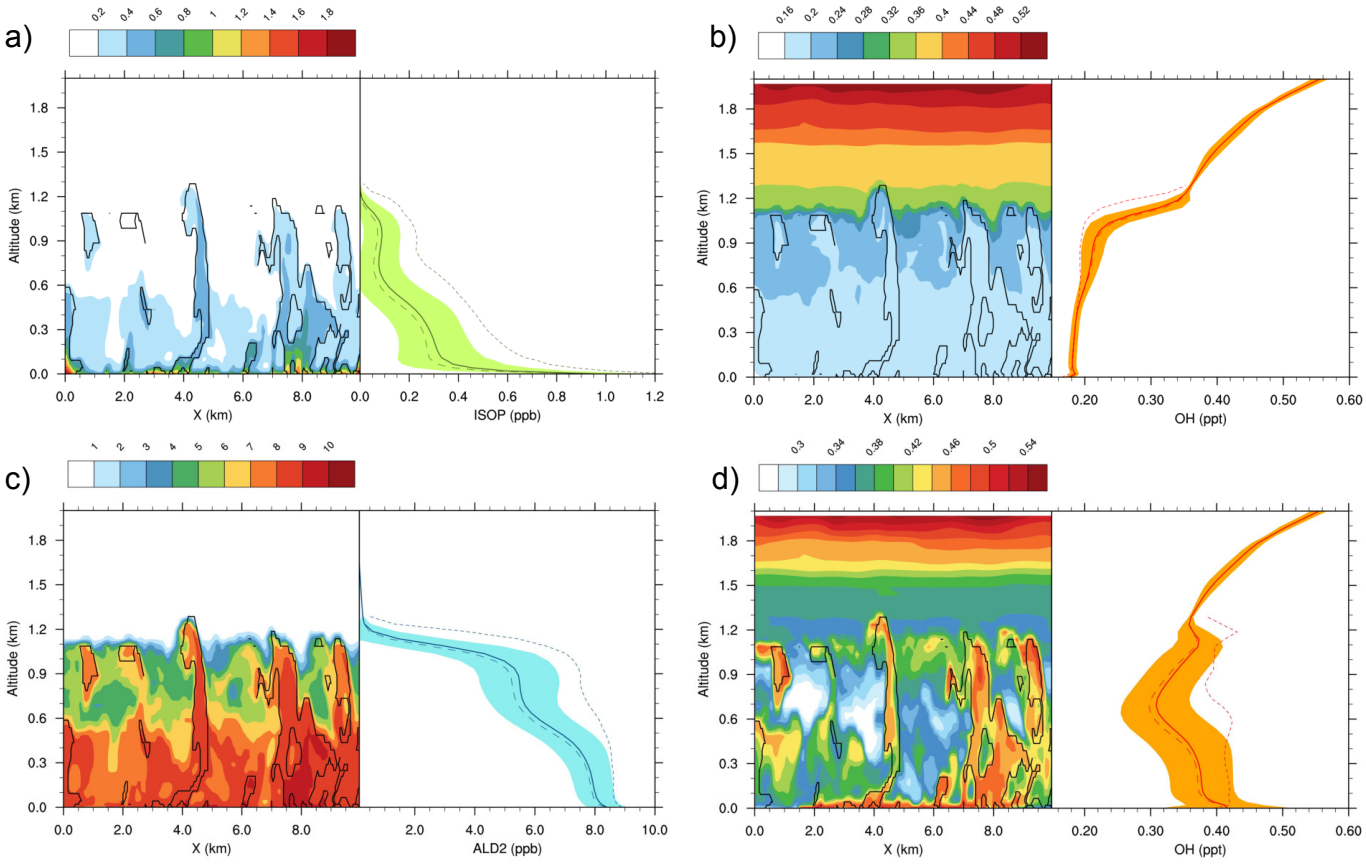

Figure 5. (a) Isoprene (ppb) and (b) OH radical (ppt) mixing ratios for the biogenic case at 1200 UTC. (c) ALD2 (ppb) and (d) OH radical (ppt) mixing ratios for the anthropogenic case at the same time. For each figure, the left part consists in vertical cross section at the middle of the domain (y = 5km). In the right part of each panel, the shaded areas denote two times the standard deviation at a given altitude and the line represents the horizontal average over the domain. The dashed line correspond to the average in the environment and the dotted lines inside thermals.

Atmos. Chem. Phys. Discuss., https://doi.org/10.5194/acp-2017-969
Manuscript under review for journal Atmos. Chem. Phys.
Discussion started: 20 November 2017

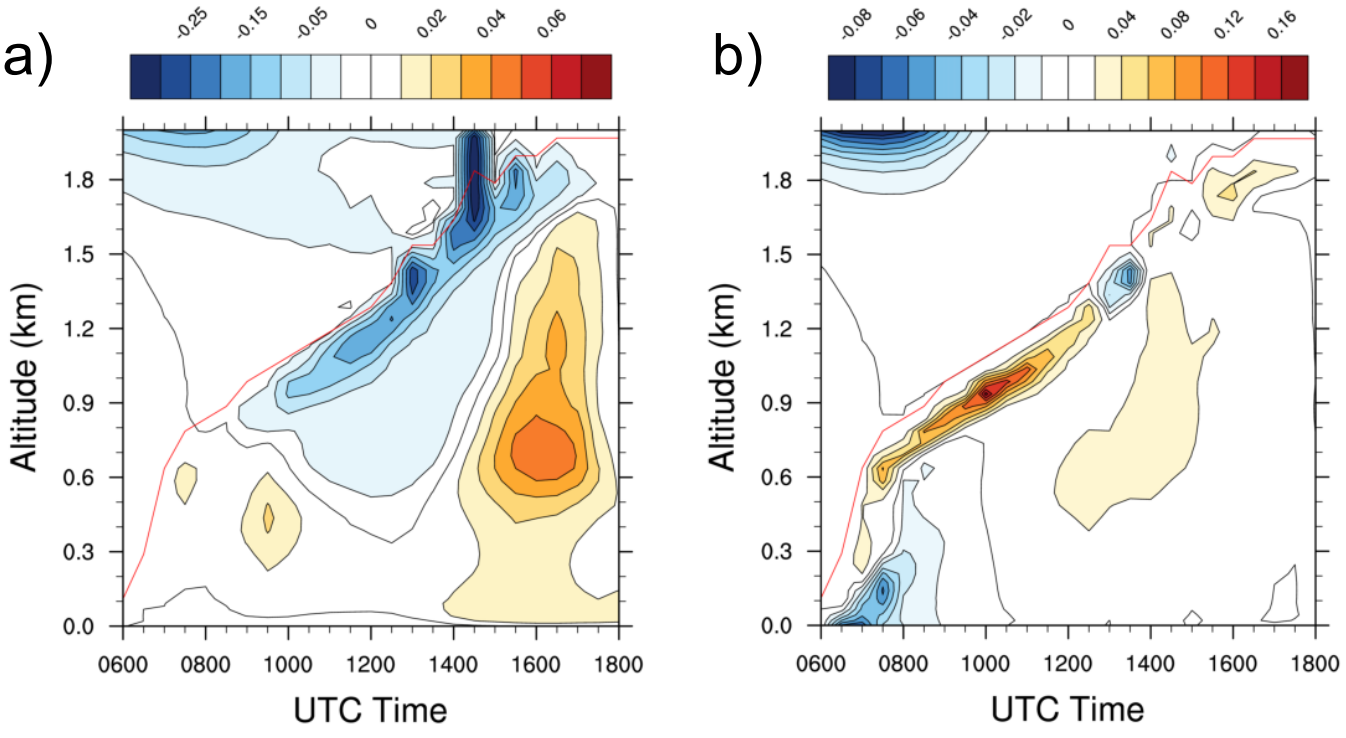

Figure 6. (a) Diurnal evolution of the segregation coefficient for isoprene and OH in the biogenic case and (b) for ALD2 and OH in the anthropogenic case. The red line represents the boundary layer height as determined by the tracer approach.

Atmos. Chem. Phys. Discuss., https://doi.org/10.5194/acp-2017-969
Manuscript under review for journal Atmos. Chem. Phys.
Discussion started: 20 November 2017

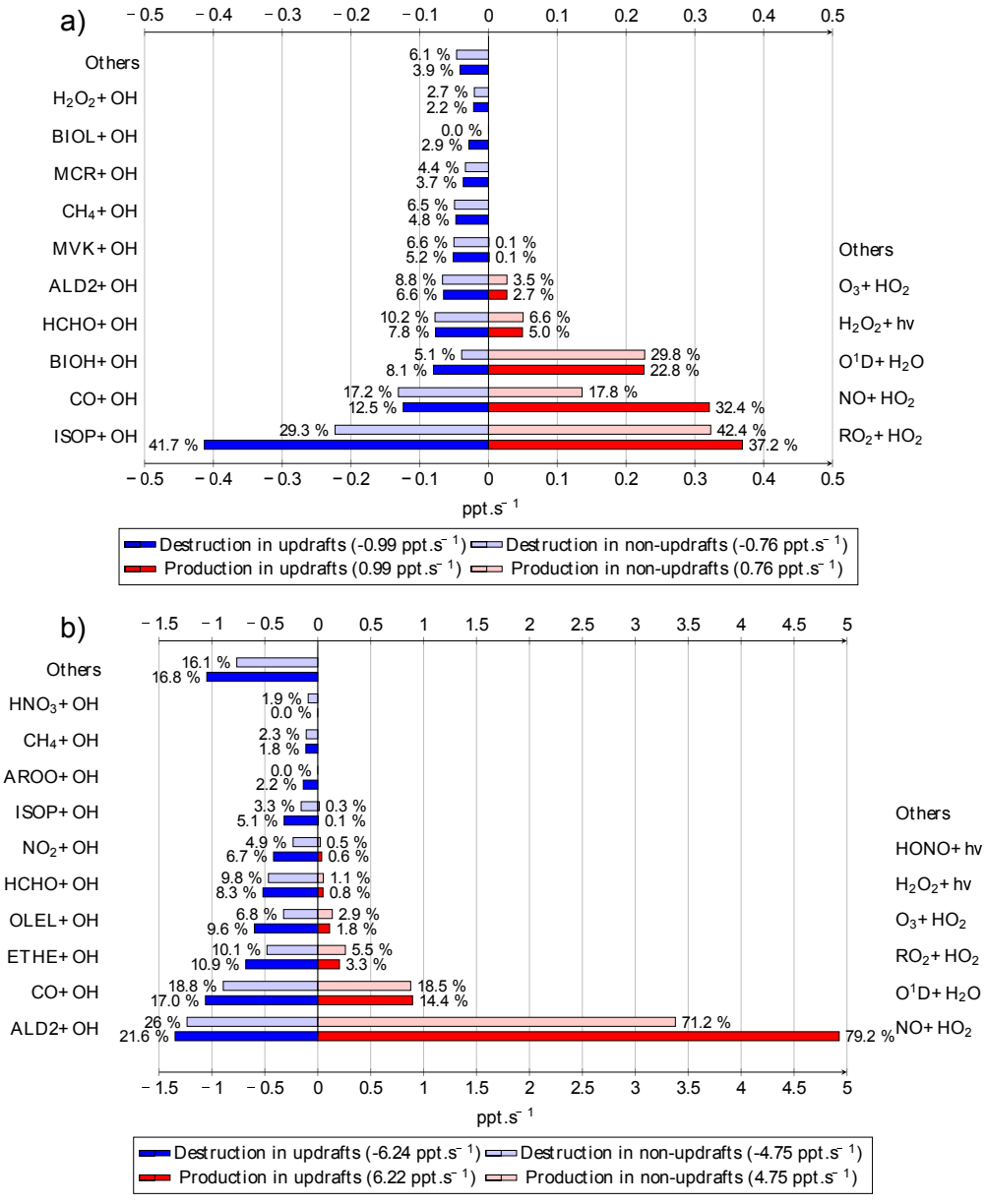

Figure 7. OH radical chemical budget at 1200 UTC averaged at 20 m for the biogenic (a) and the anthropogenic case (b). Source terms are in red for updrafts and pale red for non-updrafts. Destruction terms are in blue for updrafts and pale blue for non-updrafts. The bar lengths determine the absolute values and the relative contributions for destruction and production are given by the percentage near each bar. Number between parenthesis in the legend box are the OH production and destruction rates in updrafts and in non-updrafts. Chemical names correspond to name given in the ReLACS 3 mechanism.

Atmos. Chem. Phys. Discuss., https://doi.org/10.5194/acp-2017-969
Manuscript under review for journal Atmos. Chem. Phys.
Discussion started: 20 November 2017

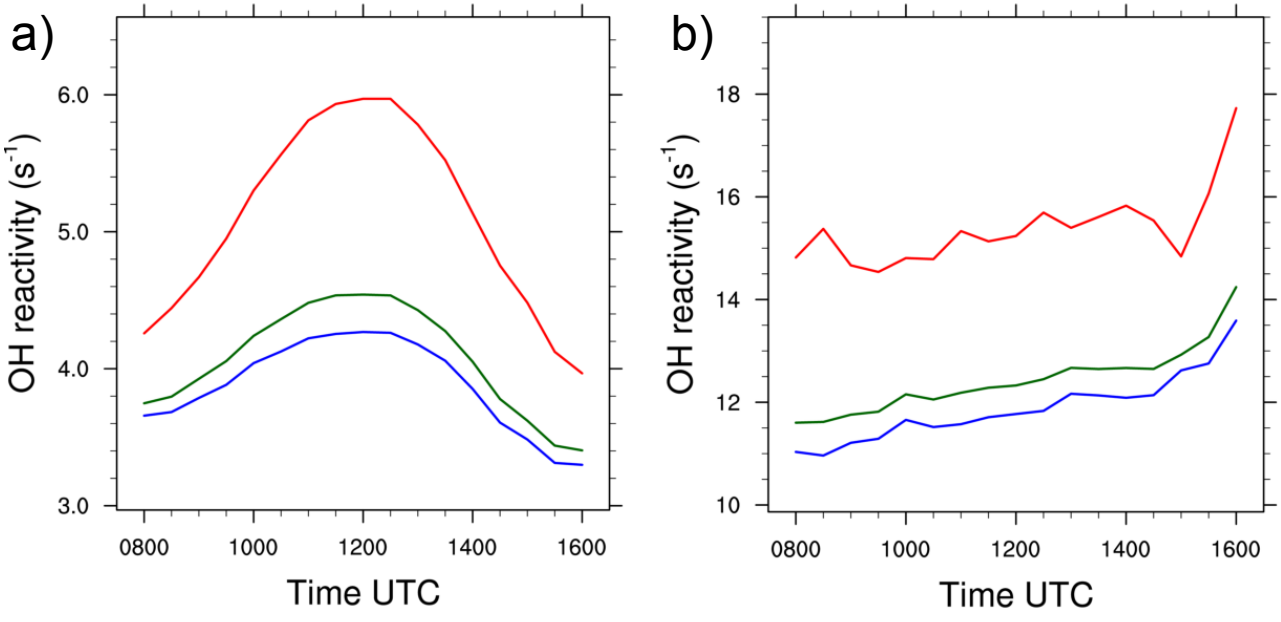

Figure 8. (a) OH reactivity (s^{-1}) in updrafts (red), domain averaged (green) and in updrafts-free region (blue) averaged at z = 20 m for the biogenic and (b) the anthropogenic case.